Insights of Electrical Engineering and Technology
https://www.achpub.com/IEET
Research Article

Experimental Demonstration and Linewidth Analysis of Dual-Cascaded All-Optical and Electro-Optical SOA-MZI Mixers for Concurrent Up and Down Frequency Mixing

Hassan Termos [1,2,*], **Kassem Kallas** [3,4,*]

[1] ICFO—The Institute of Photonic Sciences, 08860 Castelldefels, Barcelona, Spain
[2] APEX Technologies, 91460 Marcoussis, France
[3] IMT Atlantique, Inserm UMR 1101, 29200 Brest, France
[4] National Institute of Health and Medical Research, Inserm UMR 1101, 29200 Brest, France
[*] Correspondence: hassan.termos@icfo.eu (H.T.); kassem.kallas@imt-atlantique.fr (K.K.)

Received: 29 May 2026 **Revised:** 24 July 2026 **Accepted:** 14 September 2026 **Published:** 28 November 2026

Abstract: This paper presents the first experimental demonstration of a dual-cascaded semiconductor optical amplifier Mach-Zehnder interferometer (SOA-MZI) system for simultaneous up- and down-frequency mixing, comparing all-optical and electro-optical configurations under both standard and differential modulation modes. The system carries OFDM-16-QAM data at 1 GHz and produces concurrent mixed replicas at frequencies up to 235 GHz; all centered at 1550 nm. Under optimal operating conditions (input signal power of −10 dBm, optical pulse source power of 5 dBm, SOA bias current of 400 mA), the electro-optical configuration achieves a maximum simultaneous output power of 28.8 dBm and an optical conversion gain (OCG) of 38.8 dB, outperforming the all-optical configuration (23 dBm, 33 dB OCG). Beam quality measurements confirm M^2 values of 1.2 and 1.45 for the electro-optical and all-optical outputs, respectively. At a cyclic prefix of 10%, the electro-optical cascaded system achieves error vector magnitude (EVM) values of 10% and 12% for down- and up-conversion approximately 6% lower than the all-optical counterpart and supports OFDM-1024-QAM transmission at 6.96 Gbit/s with EVM below 1%. As a novel contribution, the spectral linewidths of all four cascaded configurations (all-optical standard, all-optical differential, electro-optical standard, and electro-optical differential) are characterized using a self-interferometric method across modulation frequencies from 50 MHz to 1 GHz. Linewidth is found to broaden with modulation frequency in all cases, driven by carrier density fluctuations and refractive index variations within the SOA-MZI. The electro-optical differential configuration achieves the narrowest linewidth of 80 kHz at 1 GHz, the lowest value reported for any cascaded SOA-MZI mixing system, while the all-optical standard configuration exhibits the broadest response. These linewidth results provide a new frequency-stability metric for cascaded photonic mixers and confirm the superiority of the electro-optical differential design. The improved linewidth and conversion performance observed in the electro-optical differential configuration are attributed to enhanced carrier-density stabilization, reduced amplified spontaneous emission (ASE) accumulation, and mitigation of nonlinear phase fluctuations inside the cascaded SOA-MZIs. Furthermore, differential modulation improves gain symmetry between the interferometric arms, resulting in lower phase noise and enhanced frequency stability. Overall, applying differential modulation to the electro-optical cascaded system reduces harmonic distortion by more than half compared to standard mode (from 7.7% to 3.6% for up-conversion and from 6.7% to 2% for down-conversion), improves long-term power stability to 0.66% RMS, and delivers approximately 6 dB gain in electrical conversion gain (ECG) across the full mixing band. These results establish the electro-optical differential cascaded SOA-MZI architecture as a high-performance platform for broadband Radio-over-Fiber applications at millimeter-wave frequencies.

Keywords: simultaneous up and down mixing; semiconductor optical amplifier Mach-Zehnder interferometers; orthogonal frequency-division multiplexing

1. Introduction

The rapid growth of broadband wireless multimedia services, including high-definition television, cloud computing, and video conferencing, has significantly increased the demand for high-capacity Radio-over-Fiber (RoF) systems [1]. RoF technology combines the ultra-wide bandwidth and low transmission loss of optical fibers with microwave and millimeter-

Copyright: ©2026 by the authors.
https://doi.org/10.64897/ieet.2026v2i1.001
This article is an open access article distributed under the terms and conditions of the Creative Commons Attribution (CC BY) license

wave communications, providing an efficient solution for next-generation broadband wireless networks. Furthermore, the integration of wavelength division multiplexing (WDM) enables RoF systems to support multiple high-speed channels simultaneously, making them particularly attractive for future microwave photonic applications [2,3].

Among the various photonic frequency-mixing techniques, semiconductor optical amplifier Mach-Zehnder interferometers (SOA-MZIs) have attracted considerable attention because of their ability to perform high-speed all-optical signal processing through nonlinear effects such as cross-phase modulation (XPM). Consequently, SOA-MZIs have been widely employed for optical switching, wavelength conversion, photonic frequency up- and down-conversion in both all-optical and electro-optical RoF systems [4–8], and logic gate functions [9–11]. Although cascaded SOA-MZI architectures have been proposed to improve conversion efficiency and extend the operational bandwidth, previous studies have mainly focused on individual frequency conversion processes or single-stage implementations.

Despite these advances, simultaneous optical up- and down-frequency mixing using cascaded SOA-MZI architectures has received limited experimental investigation. Moreover, previous experimental studies have primarily evaluated conversion gain and transmission performance, while important characteristics such as linewidth evolution, frequency stability, beam quality, and comprehensive comparisons between all-optical and electro-optical cascaded implementations have not been reported [12–16]. Consequently, the experimental advantages and limitations of these two approaches remain insufficiently understood.

Our previous work [17] presented a simulation study of a dual-cascaded SOA-MZI architecture for simultaneous photonic frequency mixing. Building upon that study, the present work provides the first experimental validation of the cascaded architecture and introduces a novel electro-optical implementation in addition to the all-optical configuration. Unlike our previous study [17], which was limited to numerical simulations, this work experimentally compares four operating modes, namely all-optical standard, all-optical differential, electro-optical standard, and electro-optical differential, under identical operating conditions. This comprehensive comparison demonstrates that electrically modulating the SOA gain significantly improves the operating frequency range, output optical power, optical and electrical conversion gains, beam quality, transmission performance, and long-term stability. Furthermore, this work presents the first experimental linewidth characterization of cascaded SOA-MZI photonic mixers using a self-interferometric technique, providing new insight into the phase-noise behavior of these architectures.

The main contributions of this work are summarized as follows:

- We present the first experimental validation of the dual-cascaded SOA-MZI architecture previously proposed through simulation [17] for simultaneous optical up- and down-frequency mixing.
- We propose and experimentally demonstrate a novel electro-optical cascaded SOA-MZI architecture and compare it with its all-optical counterpart under both standard and differential modulation conditions.
- We provide the first comprehensive experimental comparison of four cascaded SOA-MZI configurations using output optical power, optical conversion gain, electrical conversion gain, beam quality, total harmonic distortion (THD), error vector magnitude (EVM), and long-term power stability as performance metrics.
- We experimentally characterize the linewidth evolution of all four configurations up to a modulation frequency of 1 GHz using a self-interferometric method, demonstrating a minimum linewidth of 80 kHz for the electro-optical differential configuration.
- We demonstrate compatibility with high-order OFDM modulation formats up to OFDM-1024-QAM at 6.96 Gbit/s, enabling broadband RoF transmission at millimeter-wave frequencies reaching 235 GHz.

2. Differential Modulation for All-Optical and Electro-Optical Concurrent Up- and Down-Mixing

Optical integration based on conventional modulation techniques has been explained in previous studies [17]. Differential modulation, however, consistently provides superior performance compared to traditional modulation methods, as highlighted in our earlier research efforts [12–14]. In this context, an electro-optical simultaneous mixing approach using differential modulation is developed to assess its effectiveness against all-optical simultaneous mixing.

The proposed simultaneous generation of up- and down-mixed replicas is based on a cascaded configuration of SOA-MZIs, utilizing electro-optical differential modulation. Each SOA-MZI acts as a photonic sampling mixer, relying on XPM induced by three input optical signals within the Mach-Zehnder interferometer (MZI) integrated with SOAs, as illustrated in Figure 1. Additionally, there are four optical control inputs driven by optical pulse sources (OPSs) of uniform quality,

which are converted into electrical signals, along with an original optical data signal at frequency f_1, and two output optical signals at the output port of each SOA-MZI.

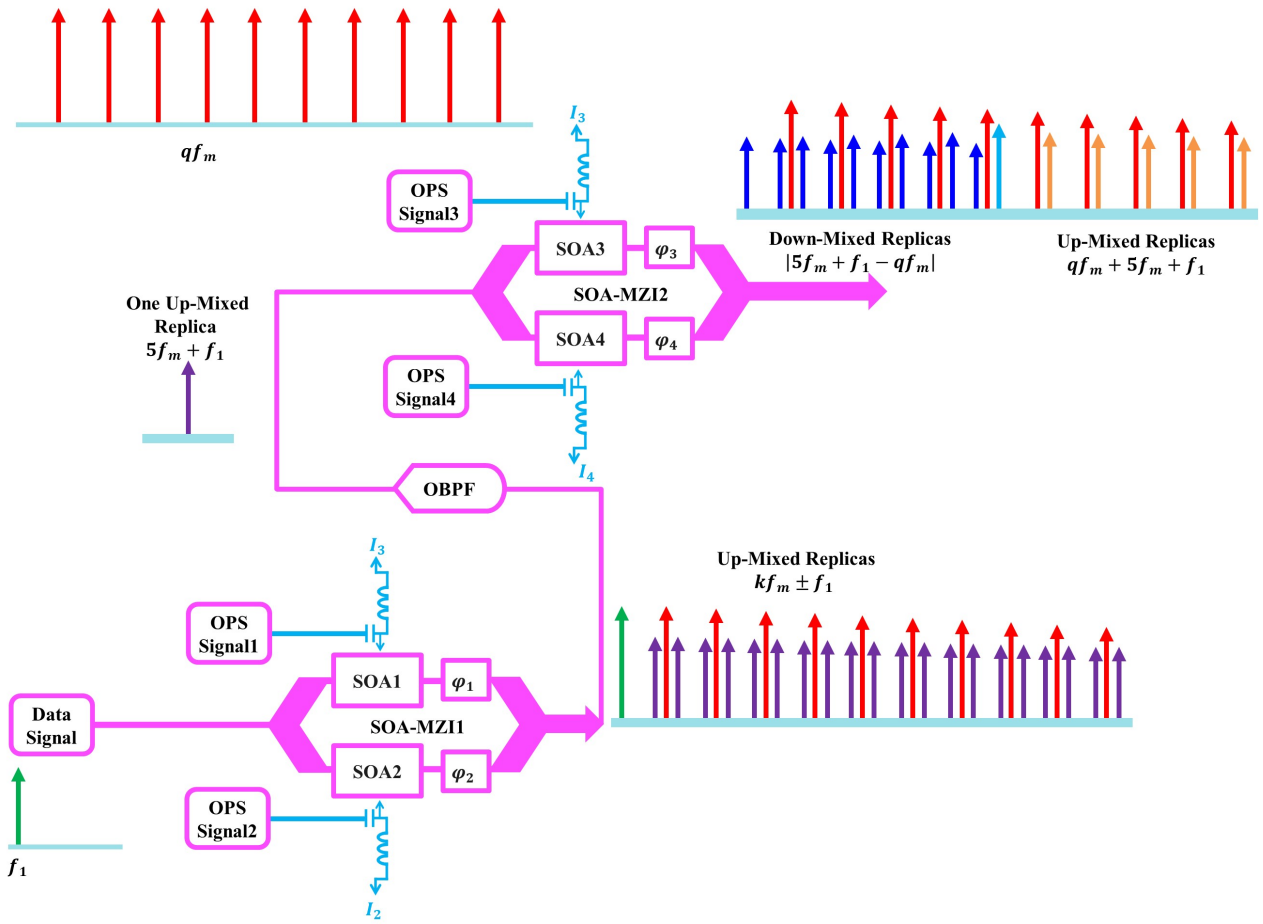


Figure 1. Electro-optical concurrent mixing principle. Blue color represents the electrical path and components while pink color represents the optical ones. The OPS harmonics have red color, the green replica is for the data signal, the violet is for the up-mixed replicas at the SOA-MZI1 output, the orange color is for the up-mixed replicas at the SOA-MZI2 output, and the blue is for the down-mixed replicas at the SOA-MZI2 output. OBPF: Optical Band-Pass Filter, SOA: Semiconductor Optical Amplifier, OPS: Optical Pulse Source, and ϕ: Phase Shifter.

In this configuration, the incoming data signal, modulated in intensity by an electrical subcarrier carrying complex modulated data at frequency f_1, is introduced into both SOAs within the first SOA-MZI (SOA-MZI1). The corresponding OPS signal, representing ultra-short clock pulses at a sampling frequency, is directed to both the upper and lower arms of the MZI associated with each SOA-MZI. As seen in the electrical spectrum of the sampling signals at the SOA electrical ports, the harmonic amplitudes vary, slightly decreasing with the harmonic order. When a sampling signal is present, the carrier density and refractive index of each SOA are modulated by the electrical control signal at the electrical gate, aided by a bias current in each arm. Consequently, the control signal modulates the data signal in each arm, causing a phase shift in the original input signal at the upper and lower outputs due to the XPM effect. This leads to the sampling of the data signal, and sampling mixers use this process for up-conversion and down-conversion [12]. The electrical spectrum of the sampled signal obtained after filtering shows replicas of the original data signal around the harmonics of the first sampling signal. These replicas at $kf_m + f_1$ have different amplitudes depending on the harmonics of the sampling signal. As a result, the data signal is up-converted to higher frequencies at the output of SOA-MZI1, where k represents an integer corresponding to the harmonic rank of the first and second control signals.

The nonlinear operation of the SOA-MZI is governed by carrier-density dynamics and XPM. The temporal carrier evolution inside each SOA can be expressed as:

$$\frac{\mathrm{d}N}{\mathrm{d}t} = \frac{I}{qV} - \frac{N}{\tau_s} - g(N)S \tag{1}$$

where N is the carrier density, I is the injection current, q is the electron charge, V is the active region volume, τ_s is the carrier lifetime, $g(N)$ is the optical gain, and S is the photon density.

The phase variation induced by gain modulation through XPM inside the SOA is expressed as:

$$\Delta\phi = -\frac{\alpha}{2}\Delta G \tag{2}$$

where α represents the linewidth enhancement factor and ΔG denotes the gain variation induced by the control signal. The induced phase shift modifies the interferometric transfer function of the SOA-MZI, enabling optical frequency mixing and harmonic replica generation.

The generated mixing frequencies at the SOA-MZI1 output are governed by:

$$f_{\text{up}} = kf_m \pm f_1 \tag{3}$$

where f_m is the optical pulse source repetition frequency, f_1 is the incoming IF data frequency, and k is the harmonic order.

For the second SOA-MZI (SOA-MZI2), which is connected in series with SOA-MZI1, a similar sampling operation is performed. However, the sampled signal at the output of SOA-MZI1, after filtering, is fed into the middle port of SOA-MZI2. An optical bandpass filter (OBPF) is used to select the desired replica of the sampled signal to be applied at the input of SOA-MZI2. The third and fourth OPS signals are applied at the electrical gates of both SOAs, and only a specific replica of the sampled signal at a higher frequency is introduced into SOA-MZI2 through the OBPF. While it is possible to inject all replicas, a deliberate choice is made to select only one to minimize the generation of excessive up- and down-converted replicas at the output of SOA-MZI2, thereby reducing output complexity.

To illustrate the principle of simultaneous up- and down-conversion, consider the sampled signal replica at $5f_s + f_1$. It is important to note that SOA-MZI2 has the same characteristics and functionality as SOA-MZI1. Due to the sampling process, the electrical spectrum at the output of SOA-MZI2 displays up-converted replicas at $qf_m \pm (5f_m + f_1)$ and down-converted replicas at $|5f_m + f_1 - qf_m|$, where q represents the harmonic order of the third and fourth sampling signals.

It is important to highlight that modulating SOAs with a RF signal that serves as the OPS signal is based on the electro-optic effect [6,16]. This process involves altering the carrier density within the SOA's semiconductor material in response to changes in the applied OPS signal. As the carrier density is adjusted, the optical signal's amplitude or phase is consequently modified. This modulation technique takes advantage of the ability to influence the gain or absorption properties of the SOA-MZI by controlling the carrier density. Alternatively, SOAs can also be modulated using an IF signal [5].

In the case of all-optical simultaneous mixing using a cascaded SOA-MZI configuration, as shown in Figure 2, the same sampling process is performed based on nonlinearities through SOA-MZI1 and SOA-MZI2. The key difference lies in the identical OPS signals introduced at the optical gate of the SOA-MZIs and the resulting all-optical concurrent replicas, which exhibit lower quality (reduced power and increased noise) compared to the electro-optical concurrent signal, as seen in the electrical spectrum at the output of SOA-MZI2 in Figure 1 and Figure 2. This outcome is influenced by the characteristics of the incoming signal and the nonlinearities of the SOA-MZI. To validate the superiority of electro-optical simultaneous mixing in terms of signal quality, both experimental and simulated results have been obtained, particularly focusing on the electrical spectrum at the output of the cascaded SOA-MZIs configuration.

The benefits of simultaneous up- and down-mixing include remote mixing capabilities, reduced weight, compact size, and the ability to handle multiple wavelengths. This transmission system, designed to generate concurrent replicas, has been studied to improve the performance of RoF systems and reduce overall system costs. However, the approach of concurrent replicas has its limitations. The most significant among these is the bandwidth limitation of both all-optical and electro-optical mixers, which restricts the effectiveness of the sampling technique and leads to the attenuation of numerous harmonics, including replicas. Another key limitation is noise, with thermal noise, jitter noise, beating noise, and noise aliasing being major sources of interference.

Electro-optical mixing within a SOA-MZI is often preferred due to its ability to achieve higher signal quality compared to all-optical mixing. This is primarily due to the benefits of integrating electrical processing stages. Utilizing the electrical ports of SOAs offers unique advantages, resulting in improved signal quality compared to an all-optical setup. While both methods experience similar nonlinear effects, such as XPM and cross-gain modulation (XGM), accessing the electrical domain enables advanced signal conditioning, noise reduction, and compensation for nonlinear distortions. By

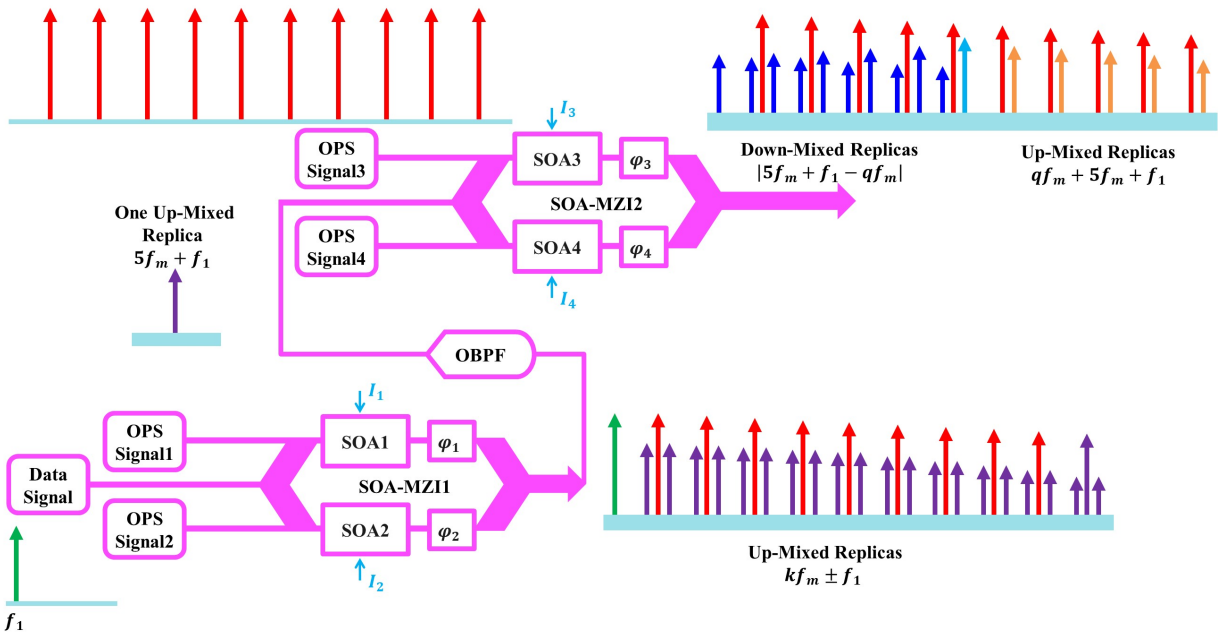


Figure 2. All-optical concurrent mixing principle.

converting the optical signal to the electrical domain, electro-optical systems can apply advanced signal conditioning techniques, like filtering and error correction, which collectively enhance signal quality. Furthermore, electro-optical systems are compatible with established electronic processing methods, allowing the use of well-developed techniques to optimize the signal and minimize noise and distortion. The flexibility of the electrical domain also permits finer control over the signal, potentially enhancing the signal-to-noise ratio (SNR).

While all-optical mixing is valued for its simplicity and speed, the advanced signal conditioning capabilities of electro-optical mixing are beneficial in situations where high signal quality is critical. However, determining which method provides better signal quality depends on specific needs and applications, as well as the operating conditions of the input signals. Both mixing techniques have their strengths, but electro-optical mixing shows advantages at higher frequencies, where maintaining signal quality is more important than speed in our system. The choice between all-optical and electro-optical mixing in a SOA-MZI ultimately depends on the specific application requirements, weighing the trade-offs between the complexity of electrical processing and the associated improvements in signal quality.

3. Experimental Configurations for All-Optical and Electro-Optical Simultaneous Up- and Down-Mixing Using Conventional Modulation

Figure 3 and Figure 4 illustrate the experimental setups for testing the mixing function using cascaded optoelectronic SOA-MZIs, with one setup designed for all-optical and the other for electro-optical configurations. Both setups utilize cascaded SOA-MZIs to evaluate up- and down-converted signals simultaneously at the output of SOA-MZI2. The experimental arrangement includes a laser source, an optical Mach-Zehnder modulator (MZM), and an initial optical attenuator (OAtt1) to generate the desired data signal. An orthogonal frequency-division multiplexing (OFDM) data carrier is produced by an arbitrary waveform generator (AWG) interfaced with the MZM, where each electrical subcarrier carries quadrature amplitude modulation (16-QAM) data at $f_1 = 1$ GHz. This data signal, with a variable average optical power at a wavelength of 1545 nm, is fed into the inlet of SOA-MZI1. The MZM operates with an electrical power of 15 dBm at its gate. The bias currents for SOA1 and SOA2 are set to 400 mA for efficient operation in each SOA-MZI. The impact of amplified spontaneous emission (ASE) noise is a key factor in evaluating the performance of both all-optical and electro-optical telecommunication systems, as it affects the characterization of each SOA [18].

The OPS [19], designed from Pritel [20], which generates a sampling signal with a pulse width of 1.3 ps and a repetition rate of $f_m = 15.6$ GHz, is set to a wavelength of $\lambda_2 = 1550$ nm. This pulse is injected into the optical control input of each SOA-MZI, as depicted in Figure 3 for the all-optical setup. In the electro-optical design, as shown in Figure 4, the OPS signal is subjected to photo-detection and amplification to obtain the electrical spectrum at each SOA-MZI's electrical port. This spectrum reveals distinct spectral components, or harmonics, $H\left(\frac{k}{q}\right)$ at frequencies of $\frac{k}{q} \times f_m$

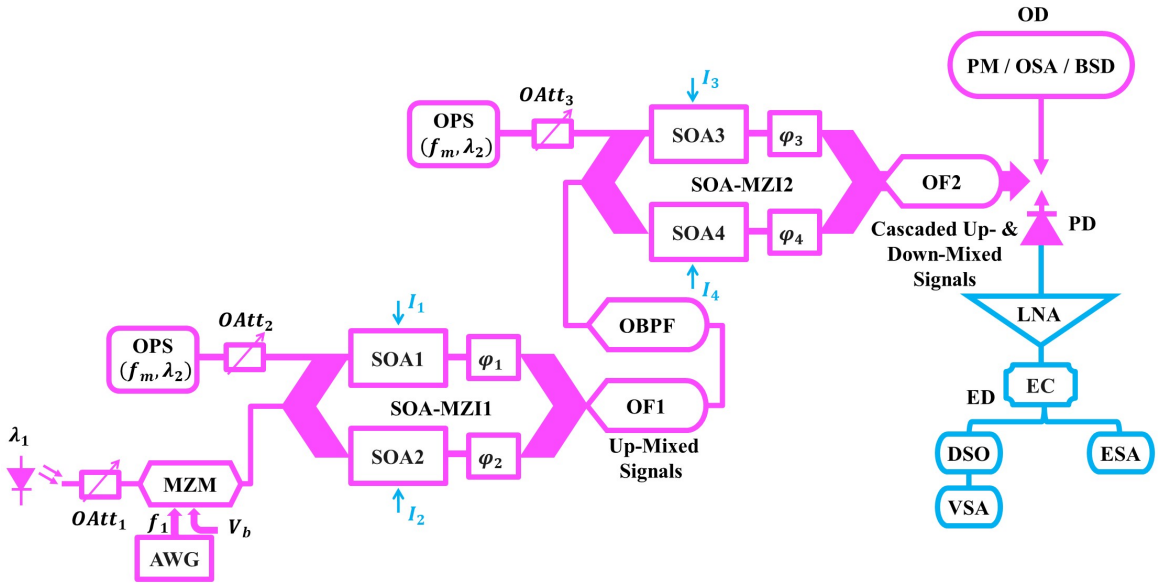


Figure 3. All-optical mixing experimental structure. LNA: Low Noise Amplifier, MZM: Mach-Zehnder Modulator, PM: Power Meter, EC: Electrical Coupler, PD: photodiode, OSA: Optical Spectrum Analyzer, ESA: Electrical Spectrum Analyzer, OD: Optical Domain, ED: Electrical Domain, BSD: Beam Squared Device, OSA: Optical Spectrum Analyzer, OF: Optical Filter, OAtt: Optical Attenuator, DSO: Digital Sampling Oscilloscope, VSA: Vector Signal Analyzer, and AWG: Arbitrary Waveform Generator.

(where $H\left(\frac{k}{q}\right) = \frac{k}{q} \times f_m$), with varying amplitudes depending on the harmonic levels k and q of the primary and secondary sampling signals, respectively. The sampling signal's peak power at the control port is typically 5 dBm, influenced by the incoming signal power, and is fed into the control gates of both SOA-MZIs.

The mixed signal emerging from each SOA-MZI is filtered using optical filters (OFs) set to the OPS signal wavelength of 1550 nm. The impact of ASE is minimal due to significant reduction by the OFs. After filtering the up-converted signal from the output of SOA-MZI1 through OF1, an optical bandpass filter (OBPF) is employed at SOA-MZI1's output to select a specific wavelength corresponding to a chosen replica of the up-converted signal. By tuning the OBPF to the wavelength of a particular replica, it selectively transmits that wavelength while blocking others. This filtered signal, now isolating the desired replica, is used as input for the SOA-MZI2. This method allows for precise manipulation and extraction of specific frequency components within the optical signal, which is crucial for applications requiring exact control and isolation of replicas. Proper selection and configuration of both the optical filter and the subsequent SOA-MZI are crucial for optimizing performance in the optical communication system.

To analyze the frequency conversion spectrum, the sampled optical carrier is detected with a 300 GHz photodiode (PD) with a sensitivity of 0.85 A/W. The signal is then amplified by a 35-dB low-noise amplifier (LNA) and analyzed using an electrical spectrum analyzer (ESA). Demodulation of the OFDM-16-QAM mixed signal is performed with a digital sampling oscilloscope (DSO) in conjunction with a vector signal analyzer (VSA), assessing various error vector magnitude (EVM) values.

Among the long-wavelength photodetectors, the uni-travelling-carrier photodetector (UTC-PD) excels with high output power across frequencies from 100 GHz to 1 THz [21,22]. This UTC-PD, designed specifically for photodetection, was extensively used in this research for frequencies exceeding 235 GHz. Its notable features, such as high-power output and a wide bandwidth with a −3 dB bandwidth reaching up to 310 GHz, made it ideal for our experimental setup [23]. However, it is important to note that the bandwidth of the ESA, specifically the 82407R model from Adler, imposes a limit on the maximum achievable frequency range, capping it at 400 GHz.

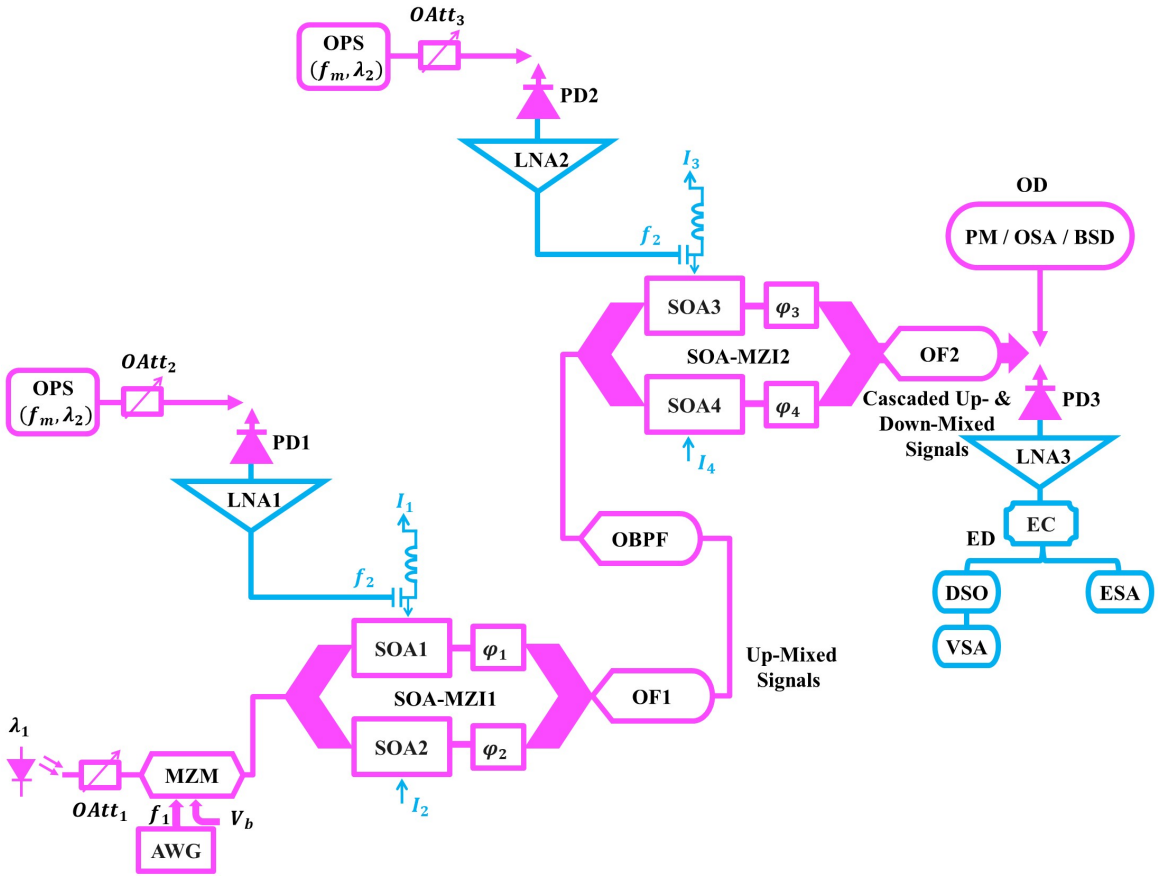


Figure 4. Electro-optical standard mixing experimental structure.

4. Evaluation of Performance for Simultaneous Up- and Down-Mixed Signals Using Conventional Modulation

4.1. Characteristics of Outgoing Optical Power, Optical Conversion Gain, and Optical Spectra

To evaluate the performance of all-optical and electro-optical configurations, the simultaneous up- and down-mixed optical signals at the output of the cascaded SOA-MZIs (the second stage) are analyzed based on output power characteristics, optical conversion gain (OCG), and optical spectra. As shown in Figure 5(a), the optical concurrent power is assessed over a range of incoming signal powers from −20 to −2 dBm, with a fixed input OPS power of 5 dBm and a constant bias current of 400 mA for all SOAs. The maximum output power achieved is 23 dBm for the all-optical configuration and 28.8 dBm for the electro-optical setup, both observed at an input power of −10 dBm. However, this output power significantly deteriorates at higher signal levels.

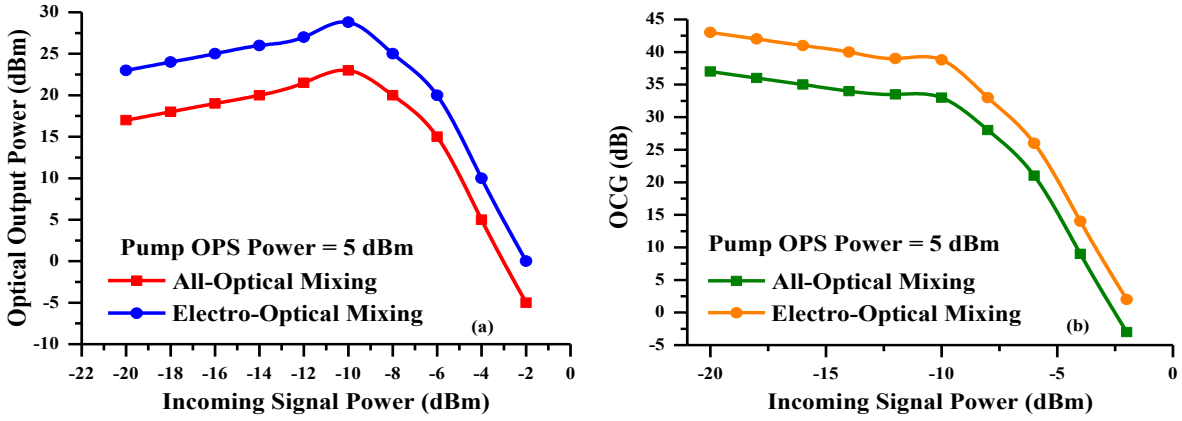


Figure 5. Output power characteristics (a) and optical conversion gain (OCG) (b) as a function of incoming signal power with a SOA bias current of 400 mA for all-optical and electro-optical cascaded designs.

The OCG is defined as the difference between the total optical output power measured at the output of the second SOA-MZI stage (SOA-MZI2) and the input optical signal power measured at the input of the first SOA-MZI stage (SOA-MZI1). As seen in Figure 5(b), the OCG for the all-optical and electro-optical cascaded systems reaches 33 dB and 38.8 dB, respectively, at −10 dBm incoming signal power. This metric is used to evaluate the overall optical amplification capability of the proposed cascaded SOA-MZI architecture. The electro-optical design exhibits a 43 dB OCG improvement in response to a significant reduction in signal power. However, although the OCG is higher at −20 dBm, this operating point is not practical for subsequent experiments because the output concurrent power decreases by up to 6 dB compared to the output power at −10 dBm [12]. This reduction is critical as it affects other mixing characteristics, particularly in the electrical domain, such as electrical conversion gain (ECG) and EVM.

Having established that the highest simultaneous output power is achieved at −10 dBm signal power and 5 dBm OPS power, further measurements of output power and OCG as a function of OPS power at −10 dBm signal power with a 400 mA SOA bias current are presented in Figure 6. Both the output power and OCG reach their maximum at 5 dBm OPS power. Despite the increase in OCG, which rises by just 10 dB across the OPS power range, this is consistent with the fixed incoming signal power of −10 dBm, as shown in Figure 6(b).

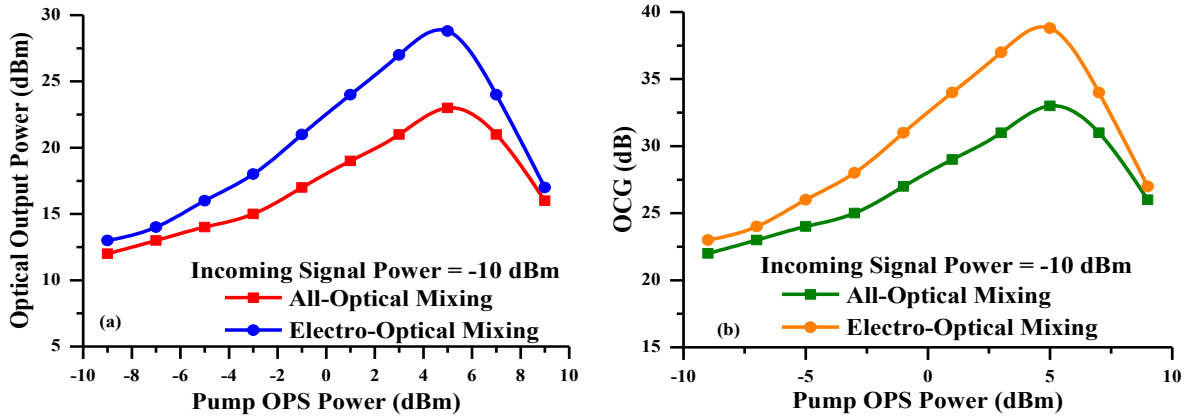


Figure 6. Output power characteristics (a) and optical conversion gain (OCG) (b) as a function of pump OPS power with a SOA bias current of 400 mA for all-optical and electro-optical cascaded setups.

The relationship between the SOA bias current and the concurrent output power at the SOA-MZI2 output for both all-optical and electro-optical cascaded configurations is depicted by the optical power versus bias current (P-I) curve in Figure 7(a). This curve shows that optical output power is relatively low at lower bias currents but increases rapidly as the SOA bias current rises. Figure 7(b) illustrates the OCG as a function of SOA bias current, highlighting that the maximum OCG is achieved at a bias current of 400 mA for both cascaded systems. Consequently, the optimal operating conditions, an incoming signal power of −10 dBm, a peak OPS power of 5 dBm, and an SOA bias current of 400 mA, are used to achieve maximum optical simultaneous powers of 23 dBm for the all-optical configuration and 28.8 dBm for the electro-optical configuration. These power levels contribute to enhanced replica powers in the electrical domain.

The degradation of optical conversion gain at high input powers is mainly associated with gain saturation inside the SOAs. As the optical carrier density increases, carrier depletion reduces the available gain recovery dynamics, resulting in compression of the nonlinear mixing efficiency. In addition, ASE accumulation and nonlinear phase fluctuations contribute to the reduction of signal quality at elevated optical powers.

In the context of a cascaded SOA-MZI link, electro-optical mixing demonstrates superior optical performance compared to all-optical mixing due to several advantageous factors. Electro-optical mixing benefits from high efficiency and rapid response times, which are crucial for effective modulation in the cascade system. The integration of electro-optical components, such as MZMs and UTC-PDs, with SOA-MZIs enhances the overall performance. This integration leverages the specific characteristics of these devices, wavelength specificity and power handling capabilities, to achieve improved signal quality and reduced noise levels. This is particularly important in cascaded systems where noise accumulation can degrade output power and signal integrity.

Upon confirming the optimal operating conditions, the optical spectra of the simultaneous up- and down-mixed signals for the all-optical and electro-optical configurations are presented in Figure 8. For the all-optical setup (Figure 8(a)), the

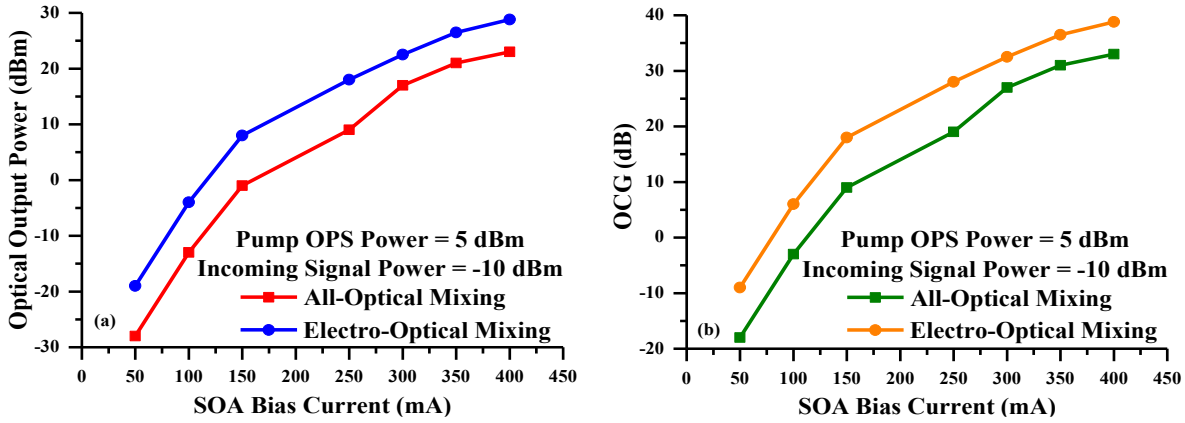


Figure 7. Output power characteristics (a) and OCG (b) as function of bias current for all-optical and electro-optical cascaded designs.

optical output power is approximately 5.8 dB lower compared to the electro-optical setup (Figure 8(b)). Despite this difference, in both cases, the noise floor remains more than 70 dB below the peak power. Given this noise level and accounting for receiver losses, the estimated simultaneous power at the SOA-MZI2 output is about 23 dBm for the all-optical configuration and 28.8 dBm for the electro-optical setup, consistent with the values reported in Figure 5, Figure 6, and Figure 7. The optical spectra show that the all-optical simultaneous signal has a bandwidth of approximately 8 nm at full width at half maximum (FWHM), whereas the electro-optical simultaneous signal exhibits a broader bandwidth of around 17 nm. Both spectra are centered at a wavelength of 1550 nm.

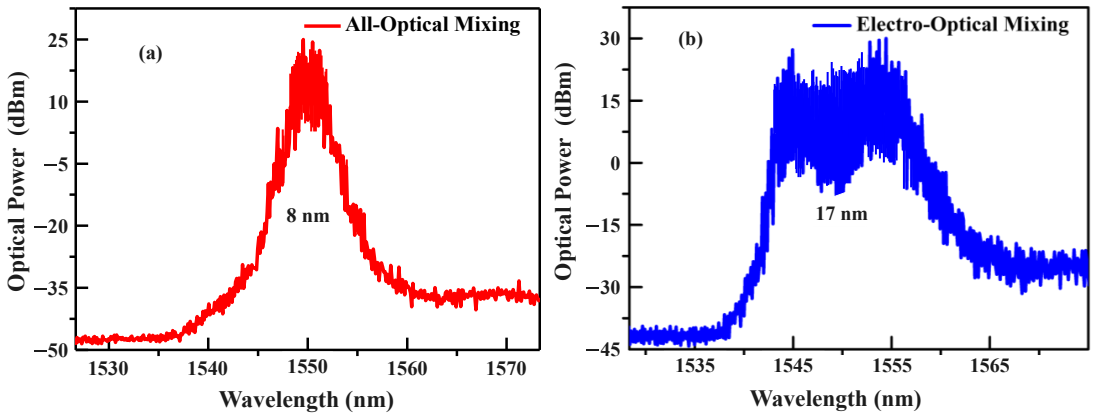


Figure 8. Optical spectrum of the all-optical (a) and Electro-Optical (b) simultaneous up- and down-mixed signal at 1550 nm.

The broader output spectrum seen in electro-optical mixing compared to all-optical mixing can be attributed to several factors. First, electro-optical mixing offers higher modulation bandwidths and faster response times, which enable more rapid changes in the optical signal. Additionally, the modulation frequency in electro-optical mixing can be higher than in all-optical systems. The interaction length, or the spatial extent of the modulation process, is also greater in electro-optical mixing, leading to a wider frequency range in the output spectrum. Finally, experimental conditions such as power levels and temperatures can affect nonlinear effects, further influencing the differences in spectral characteristics.

4.2. Beam Quality Factor

Beam quality characterization is performed to evaluate the spatial stability and propagation integrity of the generated concurrent optical replicas, particularly for free-space photonic transmission and millimeter-wave photonic antenna interfacing applications. The most important beam quality criteria are M-squared (M^2) observations, which have a unit-

less value. It is determined by comparing a laser beam's proximity to the ideal single-mode TEM00 Gaussian beam, which equals to 1 $\left(M^2 = 1\right)$. The following clarification shows how to calculate M^2 evaluations across the X direction [24,25].

$$M_x^2 = \frac{\pi D_{\min,x}^2}{2\lambda \times 2Z_{r,x}} \tag{4}$$

where $Z_r = \frac{|Z_{max} - Z_{min}|}{2}$ is the Rayleigh length, $\lambda = \lambda_2 = \lambda_2$ is the wavelength of the optical simultaneous mixed signal, D_{min} is the beam diameter at the beam radius, Z_{min} and Z_{max} are the distances where the beam diameter is $\sqrt{2}D_{min}$.

A pyroelectric camera is used to analyze the spatial beam profile in the X direction of the simultaneous signal at the SOA-MZI2 output at 1550 nm. For the all-optical architecture shown in Figure 9(a) and for the electro-optical design seen in Figure 9(b), the beam profile accentuates a single-peak Gaussian distribution and unmatched circularity of 90 and 95%, respectively.

To link the resultant SOA-MZI2 signal from the fiber into a free-space beam-squared device (BSD), it must first be collimated. Using a scanning beam profiler and an optical lens with a 120 mm focal length, the beam diameter of the simultaneous signal across the Rayleigh range is recorded. The spatial beam quality parameters, or M^2 computations, are determined to be $M_x^2 = 1.45$ for the all-optical concurrent signal and $M_x^2 = 1.2$ for the electro-optical concurrent signal by recognising the distinction in the obtained beam diameter. As demonstrated before in the OCG measurements in Figure 4 and Figure 5, as well as the optical spectrum in Figure 6, the electro-optical simultaneous output beam has exceptional quality and efficiency at the cascaded SOA-MZIs output. Because of this, its M-squared findings are superior to those of the contemporaneous all-optical signal.

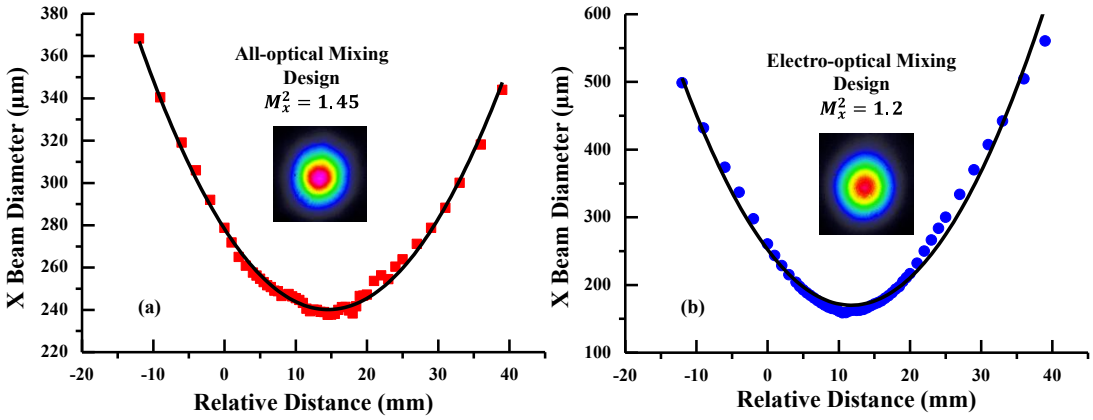


Figure 9. Evaluations of the simultaneous up- and down-mixed signal through the spatial beam profile and M-squared beam quality for all-optical cascaded design (a) and the electro-optical design (b).

Although RoF systems are predominantly fiber-based, beam quality remains an important parameter whenever free-space optical propagation, optical alignment, fiber coupling, or photonic packaging is involved. A lower M^2 value corresponds to improved beam focusing capability and coupling efficiency, thereby reducing insertion losses and contributing to improved optical power delivery and overall system stability. Consequently, the M^2 characterization complements the conversion gain and linewidth measurements by providing additional information on the optical quality of the generated signal.

4.3. Interpretation of the Frequency Replicas

The mixing frequencies associated with the generated replicas of the cascaded SOA-MZI system for simultaneous up- and down-frequency conversions are summarized in Table 1. These frequencies originate from the nonlinear interaction between the incoming OFDM optical data signal and the OPS inside the SOA-MZI structures through XPM and gain modulation mechanisms. The electrical performance of the generated concurrent up- and down-mixed signals is subsequently evaluated using the error vector magnitude (EVM) and electrical conversion gain (ECG) at the corresponding harmonic mixing frequencies.

At the input of the first SOA-MZI stage, the optical OFDM-16-QAM signal modulated at $f_1 = 1$ GHz with an average optical power of -10 dBm interacts with the OPS signal at the repetition frequency f_m. Owing to the nonlinear transfer characteristics of the SOA-MZI, multiple harmonic replicas are generated at frequencies expressed as: $f_{\text{up}} = kf_m \pm f_1$, where k represents the harmonic order generated through the nonlinear sampling process inside the SOA-MZI. The harmonic generation efficiency is governed by the carrier-density modulation dynamics and interferometric phase variation induced by the SOAs.

Table 1. Replicas frequencies of the simultaneous up- and down-mixed signals at the cascaded SOA-MZIs output. SF: Source Frequency and MF: Mixing Frequency.

SF: f_1 **(GHz)**	**Up MFs:** $kf_m + f_1$ **at SOA-MZI1 Output (GHz)**	**SF:** $5f_m + f_1$ **(GHz)**	**At SOA-MZI2 Output**	
			Up MF: $qf_m + 5f_m + f_1$ **(GHz)**	**Down MF:** $\lvert 5f_m + f_1 - qf_m \rvert$ **(GHz)**
1	$f_m + f_1 = 16.6$	79	$f_m + 5f_m + f_1 = 94.6$	$\lvert 5f_m + f_1 - f_m \rvert = 63.4$
	$2f_m + f_1 = 32.2$		$2f_m + 5f_m + f_1 = 110.2$	$\lvert 5f_m + f_1 - 2f_m \rvert = 47.8$
	$3f_m + f_1 = 47.8$		$3f_m + 5f_m + f_1 = 125.8$	$\lvert 5f_m + f_1 - 3f_m \rvert = 32.2$
	$4f_m + f_1 = 63.4$		$4f_m + 5f_m + f_1 = 141.4$	$\lvert 5f_m + f_1 - 4f_m \rvert = 16.6$
	$5f_m + f_1 = 79$		$5f_m + 5f_m + f_1 = 157$	$\lvert 5f_m + f_1 - 5f_m \rvert = 1$
	$6f_m + f_1 = 94.6$		$6f_m + 5f_m + f_1 = 172.6$	$\lvert 5f_m + f_1 - 6f_m \rvert = 14.6$
	$7f_m + f_1 = 110.2$		$7f_m + 5f_m + f_1 = 188.2$	$\lvert 5f_m + f_1 - 7f_m \rvert = 30.2$
	$8f_m + f_1 = 125.8$		$8f_m + 5f_m + f_1 = 203.8$	$\lvert 5f_m + f_1 - 8f_m \rvert = 45.8$
	$9f_m + f_1 = 141.4$		$9f_m + 5f_m + f_1 = 219.4$	$\lvert 5f_m + f_1 - 9f_m \rvert = 61.4$
	$10f_m + f_1 = 157$		$10f_m + 5f_m + f_1 = 235$	$\lvert 5f_m + f_1 - 10f_m \rvert = 77$

At the output of the first SOA-MZI stage, the up-converted component corresponding to $5f_m + f_1 = 79$ GHz is selected using an optical bandpass filter (OBPF) [17]. This selected harmonic replica serves as the optical input signal for the second cascaded SOA-MZI stage. The second stage further enhances the nonlinear mixing process through successive harmonic interactions, producing simultaneous up-converted and down-converted replicas at frequencies given by: $qf_m \pm 5f_m + f_1$ and $|5f_m + f_1 - qf_m|$, where q denotes the harmonic order generated by the second SOA-MZI stage. Consequently, the cascaded arrangement enables simultaneous frequency multiplication and frequency translation over a broad operational range. The successive nonlinear interactions inside the cascaded SOA-MZIs significantly extend the achievable mixing frequencies while preserving the integrity of the OFDM signal.

The effectiveness of the cascaded mixing mechanism is strongly influenced by the carrier recovery time, gain saturation dynamics, and phase modulation efficiency of the SOAs. At elevated harmonic orders, the conversion efficiency gradually decreases because of reduced carrier modulation bandwidth and amplified spontaneous emission (ASE) accumulation within the cascaded amplification stages. Nevertheless, the cascaded electro-optical differential configuration demonstrates enhanced harmonic generation efficiency and improved spectral stability compared with the all-optical arrangement due to its improved gain symmetry and reduced nonlinear distortion accumulation.

4.4. Electrical Conversion Gain

The electrical spectrum attributes of up- and down-mixing at the SOA-MZI2 output are described [17] for different ranges of mixing frequencies. We can observe the degradation of the electrical output power as well as the electrical conversion gain (ECG) for up- and down-mixed signals with the increase of the mixing frequency, as seen in Table 2.

The down ECG is superior to the up ECG because it has a lower mixing frequency. This improvement is due to the low-pass nature of the applied SOA-MZIs. The highest ECG of the up-mixed signal is 4.3 dB, while it is 8.4 dB for the down-converted signal. Furthermore, the maximum frequency range is 235 and 77 GHz for up- and down-shifting, respectively. The features of the electro-optical cascaded concept are also acquired, as displayed in The reduction in ECG at higher mixing frequencies is primarily linked to the finite SOAs carrier recovery time and the low-pass nonlinear response of the SOA-MZI. As the modulation frequency approaches and exceeds the effective carrier dynamics bandwidth, the nonlinear gain modulation efficiency reduces significantly, resulting in attenuation of higher-order harmonic replicas.

Table 3. In comparison to the all-optical method, the ECG of the up- and down-conversion dependent on the electro-optical system improves by an average of 6 dB throughout the whole band of the mixing frequency. This advancement stems from fine-tuning signal power to alleviate both noise and distortions. The reduction in ECG at higher mixing

Table 2. Electrical features of the cascaded SOA-MZIs system for the all-optical concept.

Electrical Characteristics at SOA-MZI2 Output All-Optical Concept					
Up Mixing at $qf_m+5f_m+f_1$			**Down Mixing at $\lvert 5f_m+f_1-qf_m\rvert$**		
Mixing Frequency (GHz)	**Power (dBm)**	**ECG (dB)**	**Mixing Frequency (GHz)**	**Power (dBm)**	**ECG (dB)**
$f_m+5f_m+f_1=94.6$	−22.2	4.3	$\lvert 5f_m+f_1-f_m\rvert=63.4$	−18.1	8.4
$2f_m+5f_m+f_1=110.2$	−24.5	2	$\lvert 5f_m+f_1-2f_m\rvert=47.8$	−20.2	6.3
$3f_m+5f_m+f_1=125.8$	−27.6	−1.1	$\lvert 5f_m+f_1-3f_m\rvert=32.2$	−23.4	3.1
$4f_m+5f_m+f_1=141.4$	−31.2	−4.7	$\lvert 5f_m+f_1-4f_m\rvert=16.6$	−27.1	−0.6
$5f_m+5f_m+f_1=157$	−36.5	−10	$\lvert 5f_m+f_1-5f_m\rvert=1$	−31.2	−4.7
$6f_m+5f_m+f_1=172.6$	−41.1	−14.6	$\lvert 5f_m+f_1-6f_m\rvert=14.6$	−37	−10.5
$7f_m+5f_m+f_1=188.2$	−46.4	−19.9	$\lvert 5f_m+f_1-7f_m\rvert=30.2$	−42.1	−15.6
$8f_m+5f_m+f_1=203.8$	−52.1	−25.6	$\lvert 5f_m+f_1-8f_m\rvert=45.8$	−48.2	−21.7
$9f_m+5f_m+f_1=219.4$	−58.3	−31.8	$\lvert 5f_m+f_1-9f_m\rvert=61.4$	−54	−27.5
$10f_m+5f_m+f_1=235$	−66.2	−39.7	$\lvert 5f_m+f_1-10f_m\rvert=77$	−61.9	−35.4

frequencies is primarily linked to the finite SOAs carrier recovery time and the low-pass nonlinear response of the SOA-MZI. As the modulation frequency approaches and exceeds the effective carrier dynamics bandwidth, the nonlinear gain modulation efficiency reduces significantly, resulting in attenuation of higher-order harmonic replicas.

Table 3. Electrical attributes of the cascaded SOA-MZIs arrangement for the electro-optical cascaded proposal.

Electrical Characteristics at SOA-MZI2 Output for Electro-Optical Concept					
Up Mixing at $qf_m+5f_m+f_1$			**Down Mixing at $\lvert 5f_m+f_1-qf_m\rvert$**		
Mixing Frequency (GHz)	**Power (dBm)**	**ECG (dB)**	**Mixing Frequency (GHz)**	**Power (dBm)**	**ECG (dB)**
$f_m+5f_m+f_1=94.6$	−16.2	10.3	$\lvert 5f_m+f_1-f_m\rvert=63.4$	−12	14.5
$2f_m+5f_m+f_1=110.2$	−18.4	8.1	$\lvert 5f_m+f_1-2f_m\rvert=47.8$	−14.2	12.3
$3f_m+5f_m+f_1=125.8$	−21.6	4.9	$\lvert 5f_m+f_1-3f_m\rvert=32.2$	−17.3	9.2
$4f_m+5f_m+f_1=141.4$	−25	1.5	$\lvert 5f_m+f_1-4f_m\rvert=16.6$	−21	5.5
$5f_m+5f_m+f_1=157$	−31.2	−4.7	$\lvert 5f_m+f_1-5f_m\rvert=1$	−25.6	0.9
$6f_m+5f_m+f_1=172.6$	−35.2	−8.7	$\lvert 5f_m+f_1-6f_m\rvert=14.6$	−31.5	−5
$7f_m+5f_m+f_1=188.2$	−40.9	−14.4	$\lvert 5f_m+f_1-7f_m\rvert=30.2$	−36.5	−10
$8f_m+5f_m+f_1=203.8$	−46	−19.5	$\lvert 5f_m+f_1-8f_m\rvert=45.8$	−42.2	−15.7
$9f_m+5f_m+f_1=219.4$	−52.2	−25.7	$\lvert 5f_m+f_1-9f_m\rvert=61.4$	−48.5	−22
$10f_m+5f_m+f_1=235$	−60.1	−33.6	$\lvert 5f_m+f_1-10f_m\rvert=77$	−55.2	−28.7

4.5. Error Vector Magnitude

The error vector magnitude (EVM) [26] of the concurrent mixed OFDM transmission at the SOA-MZI2 output is measured over a complete range of the cyclic prefix (CP) for all-optical and electro-optical cascaded mixing systems for up-conversion at $f_m+5f_m+f_1=94.6$ GHz and down-conversion at $\lvert 5f_m+f_1-f_m\rvert=63.4$ GHz, as shown in Figure 10. The OFDM format includes 128 subcarriers, with 98 of them containing 16-QAM data [12]. At a CP of 10%, the most desirable EVM values of the contemporaneous up- and down-mixed signal are 12 and 10% for the electro-optical notion, respectively. This range is increased by 6% for up- and down-conversions in the all-optical proposal. The enlargement of the EVM amounts for both implementations reduces the performance transmission of the cascaded mixing system as the CP increases. It is critical to realize that each CP has a symbol rate (SR) along with a bit rate (BR) [12], as shown in Table 4.

The improved EVM performance obtained in the electro-optical differential configuration is attributed to enhanced suppression of nonlinear distortions, reduced ASE-induced phase noise, and improved balance between the interferometric arms of the cascaded SOA-MZIs. In addition, differential modulation reduces harmonic distortion and stabilizes the gain dynamics of the SOAs, thereby improving OFDM constellation integrity.

https://doi.org/10.64897/ieet.2026v2i1.001

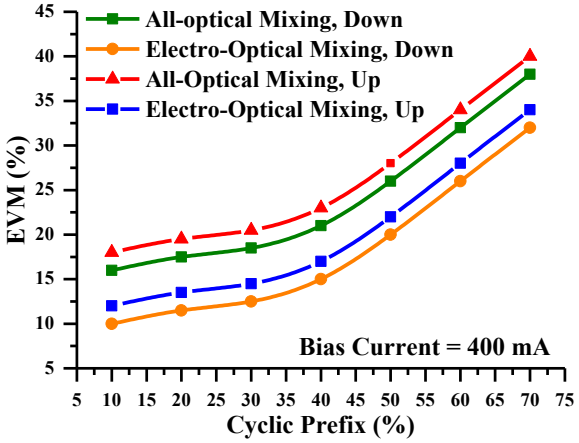


Figure 10. EVM vs cyclic prefix for both all-optical and electro-optical cascaded systems in the case of 16-QAM-OFDM up- and down-mixing.

Table 4. Results of SR and BR calculations of the OFDM-16-QAM mixed signal using at the SOA-MZI2 outlet.

CP (%)	SR (Gsymb/s)	BR (Gbit/s)
10	0.45	1.39
20	0.42	1.28
30	0.39	1.18
40	0.36	1.09
50	0.33	1.02
60	0.31	0.96
70	0.29	0.90

5. Electro-Optical Cascaded Systems Using Differential and Standard Modulation Modes

In the previous findings shown above, we gave a performance assessment of the standard electro-optical cascaded setup. Figure 4 is adjusted for differential mode, which consistently produces better results than standard mode [27,28], by inserting an additional OPS signal at the electrical side of each lower SOA within each SOA-MZI, as shown in Figure 11. The precise notion of differential configuration and its benefits are expounded in [12].

Table 5 shows the operating points that correlate to being identical for electro-optical differential and standard designs according to cascading two SOA-MZIs. This table contains the bias current of the two SOAs inside each SOA-MZI, $I_1 = I_2$, the wavelength of the OPS signal λ_2, the wavelength of the data signal λ_1, the average power of the data signal P_1, the peak power of the OPS signal P_2, the CP of the OFDM data signal, the number of data subcarriers N_d, the data frequency f_1, the OPS frequency f_m, and the wavelength of both optical filters regulated at $\lambda_3 = \lambda_2$.

Table 5. Operational parameters set for electro-optical differential and standard architectures.

Parameters	Values
$I_1 = I_2$ (mA)	400
λ_2 (nm)	1550
λ_1 (nm)	1545
P_1 (dBm)	−10
P_2 (dBm)	5
CP (%)	10
N_d	98
f_1 (GHz)	1
f_m (GHz)	15.6
λ_3 (nm)	1550

Four metrics are used to assess and compare the performance of the electro-optical differential and standard schemes based on the two cascaded SOA-MZIs:

- The power stability at the output of the second stage over one hour.
- The ECG as a function of the electrical power at the MZM electrical gate.

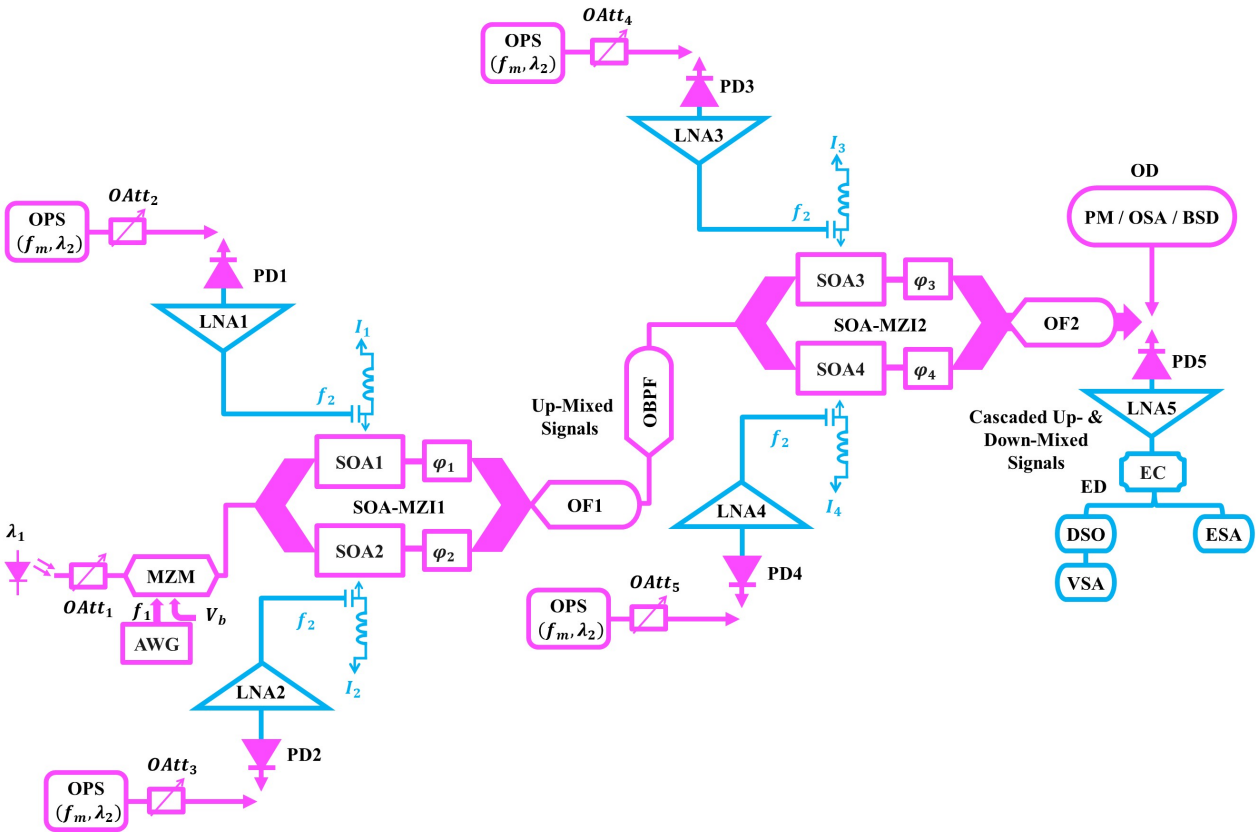


Figure 11. Experimental arrangement of the differential electro-optical cascaded system, the only difference in comparison to Figure 4 is adding another OPS signal at the lower SOA of each SOA-MZI.

- The harmonic distortion obtained for the first harmonic and its frequency components of the simultaneous up- and down-converted signal.
- The EVM as function of several number of bits that corresponds to a variety of data transmission formats, OFDM-M-QAM, at a fixed CP.

The power stability of a potent and effective system demonstrates its capacity for preserving operative harmony. The key feature of the concurrent up- and down-mixed signal at the SOA-MZI2 outcome, as seen in Figure 12, is its long-term power stability, which is obtained from the differential and standard electro-optical mixing modes. Over one hour, the output simultaneous power is calculated to overture advantageous passive stability of approximately 0.66% RMS (Root Mean Square) for the differential approach and 1.5% RMS for the standard regime to perform all experimental tests of the electro-optical mixing systems. These results prove a minimal variation in output power, which is excellent for assessing our cascade systems. It is worth repeating that the concurrent up- and down-mixed signal was processed at the SOA-MZI outlet at the 1550 nm wavelength.

The ECG is also recorded for the differential and standard electro-optical cascaded designs for various electrical powers injected at the MZM electrical gate. It was previously obtained for the standard layout at 15 dBm MZM electrical power. As the MZM electrical power increases, so does the output electrical power and the ECG for the concurrent up- and down-converted signal. The differential design enhances the overall system by around 6 dB for up- and down-conversions, as shown in Figure 13.

Differential modulation improves the cascaded SOA-MZI performance by introducing symmetrical carrier modulation in both interferometric arms. This balanced operation minimizes phase mismatch, suppresses residual chirp, and reduces nonlinear distortion accumulation. Consequently, the differential mode enhances conversion efficiency while simultaneously improving signal stability and linewidth performance.

The harmonic distortion analysis in this work is performed on the converted signal generated at the output of the second SOA-MZI stage. The reported distortion metric is calculated from the dominant second- and third-order harmonic components of the converted signal relative to its fundamental component, since these were the dominant nonlinear products observed experimentally within the measurement bandwidth.

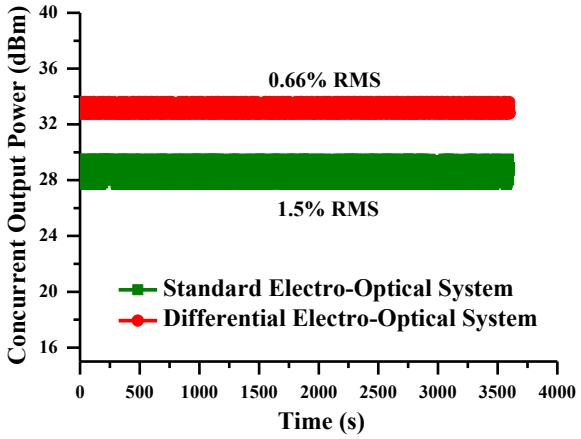


Figure 12. Power stability of differential and standard electro-optical cascaded systems.

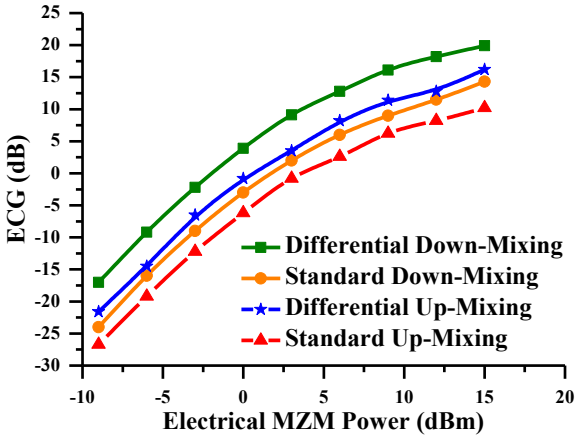


Figure 13. ECG of differential and standard electro-optical cascaded systems for different electrical powers inject at the MZM electrical gate.

For the proposed cascaded electro-optical system, the harmonic distortion analysis is performed with respect to the converted output signal. The fundamental component corresponds to the desired up- or down-converted signal, while the second- and third-order harmonic components are measured at frequencies shifted by $2f_1$ and $3f_1$ of the data signal, respectively, from the converted component. These dominant harmonic components are used to evaluate the nonlinear distortion introduced by the cascaded SOA-MZI mixer. In this work, the distortion metric is calculated from the dominant second- and third-order harmonic components relative to the fundamental converted signal. For up-conversion, the fundamental component is located at $qf_m+5f_m+f_1=94.6$ GHz, while the second- and third-order harmonic components are located at $qf_m+5f_m+2f_1=95.6$ GHz and $qf_m+5f_m+3f_1=96.6$ GHz, respectively. Similarly, for down-conversion, the fundamental component is located at $|5f_m+f_1-qf_m|=63.4$ GHz, whereas the second- and third-order harmonic components appear at $|5f_m+2f_1-qf_m|=64.4$ GHz and $|5f_m+3f_1-qf_m|=65.4$ GHz, where q is 1.

According to the standard definition [29], The harmonic distortion is evaluated by calculating the ratio between the total generated harmonic power and the fundamental output power as defined in the equations (5) and (6). In the present work, only the dominant second- and third-order harmonic components of the converted signal were experimentally measured and analyzed.

$$\mathrm{HD_{up}}=\frac{P_{qf_m+5f_m+2f_1}+P_{qf_m+5f_m+3f_1}}{P_{qf_m+5f_m+f_1}},\ q=1 \tag{5}$$

$$\mathrm{HD_{down}}=\frac{P_{|5f_m+2f_1-qf_m|}+P_{|5f_m+3f_1-qf_m|}}{P_{|5f_m+f_1-qf_m|}},\ q=1 \tag{6}$$

Table 6 summarizes the harmonic distortion of the converted signals for the standard and differential electro-optical cascaded SOA-MZI configurations. The distortion was evaluated from the dominant second- and third-order harmonic

components relative to the corresponding fundamental converted signal for both the up- and down-conversion processes. For the standard electro-optical cascaded configuration, the harmonic distortion reaches **7.7%** for the up-converted signal and **6.7%** for the down-converted signal, indicating a higher contribution of nonlinear harmonic components generated during the frequency conversion process. By applying the proposed differential electro-optical configuration, the harmonic distortion is significantly reduced to **3.6%** for up-conversion and **2.0%** for down-conversion. This corresponds to reductions of approximately **53%** and **70%**, respectively, compared with the standard configuration. The reduced harmonic distortion demonstrates that the differential modulation scheme effectively suppresses the dominant nonlinear harmonic components generated by the cascaded SOA-MZI architecture. Consequently, the converted signals exhibit improved spectral purity and reduced nonlinear distortion, making the proposed differential electro-optical configuration more suitable for high-quality Radio-over-Fiber transmission.

Table 6. Total harmonic distortion, THD (%), for the standard and differential electro-optical cascaded systems.

Standard		**Differential**	
Up	**Down**	**Up**	**Down**
7.7	6.7	3.6	2

The comparison between differential and standard electro-optical cascaded systems is achieved for a variety of OFDM-M-QAM data related to different bit numbers n, as given in Table 7. Even if the symbol rate and bandwidth of the OFDM signal remain constant, changing n causes alterations in the BR amounts as well as the data modulation forms, as shown in Table 7 [12]. The EVM of the mixed OFDM-M-QAM signal is measured at the target frequency of 94.6 GHz for up-conversion and 63.4 GHz for down-conversion at a symbol rate of 0.91 Gsymb/s at a CP of 10%. The EVM decreases from 13% at $n = 2$ related to the mixed OFDM-4-QAM signal to 0.25 % at $n = 10$ linked to the mixed OFDM-1024-QAM signal for the differential down electro-optical cascaded system, while it decreases from 18 to 1.5% for the standard down electro-optical cascaded arrangement, as illustrated in Figure 14.

For the differential up electro-optical cascaded design, the EVM reaches 1% at $n = 10$, while it is 2% for the standard up electro-optical cascaded approach. The EVM of the forward error correction (FEC) limit varies for different QAM data formats [30–33] ranging from 17.5 % for 4-QAM to 1.8% for 1024-QAM. Therefore, the differential mode optimizes more the performance of the electro-optical cascaded system, with exceptional findings related to demodulation of the mixed OFDM-1024-QAM signal with an EVM value less than 1% at the BR of 6.96 Gbit/s.

The EVM values reported in this work were obtained using the Agilent 89600 Vector Signal Analyzer (VSA) after OFDM synchronization, channel estimation, and adaptive equalization. Each modulation format (4-, 8-, 16-, 32-, 64-, 128-, 256-, 512-, and 1024-QAM) was analyzed independently using its corresponding optimized receiver configuration. Therefore, the reported EVM values should not be interpreted as the performance of different modulation orders under identical transmission conditions, but rather as the measured quality achieved for each optimized modulation format. The measured EVM values are compared with their corresponding FEC thresholds [30–33] to verify the feasibility of high-order OFDM transmission. The same VSA-based measurement methodology has been previously validated in our experimental study on concurrent M-QAM transmission [4].

Table 7. Outcomes of BR of the OFDM mixed signal using M-QAM Modulation Format at the SOA-MZI2 outlet at a fixed SR of 0.91 Gsymb/s.

Number of bits n	**M-QAM**	**BR (Gbit/s)**
2	4-QAM	1.39
3	8-QAM	2.09
4	16-QAM	2.78
5	32-QAM	3.48
6	64-QAM	4.18
7	128-QAM	4.87
8	256-QAM	5.57
9	512-QAM	6.26
10	1024-QAM	6.96

https://doi.org/10.64897/ieet.2026v2i1.001

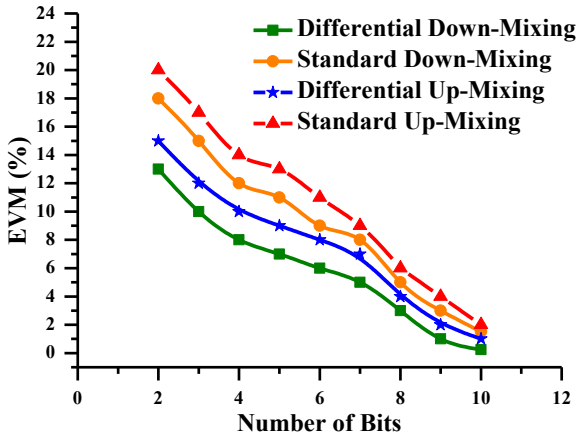


Figure 14. EVM measurements of the electro-optical cascaded systems using standard and differential modes for up- and down-conversions.

6. All-Optical and Electro-Optical Mixing Replicas Using Differential Modulation Mode

In this section, we undertake a comparison between all-optical and electro-optical mixing replicas utilizing the differential modulation mode. This comparison aims to validate the principles expounded in the second section, with a particular focus on assessing the efficacy of the electrical spectrums at the output of SOA-MZI2. By scrutinizing the outcomes obtained through this comparative analysis, we seek to further affirm the principles elucidated earlier, specifically in the context of differential modulation. The electrical spectrums at the output of SOA-MZI2 will serve as crucial indicators in evaluating the performance disparities between the all-optical and electro-optical mixing approaches in this particular modulation mode. This comparative assessment will contribute to a comprehensive understanding of the strengths and limitations inherent in each approach, ultimately bolstering the validation of the proposed principles.

In the preceding configurations presented above, we conducted a performance evaluation of both all-optical and electro-optical systems utilizing standard modulation in Figure 3 and Figure 4, respectively. The performance assessment for the electro-optical differential mode setup has also been scrutinized, as illustrated in Figure 11. Figure 15 delineates the arrangement for all-optical replicas employing differential modulation, constituting the fourth setup designed to distinguish between electro-optical and all-optical mixing, as well as standard and differential modulations.

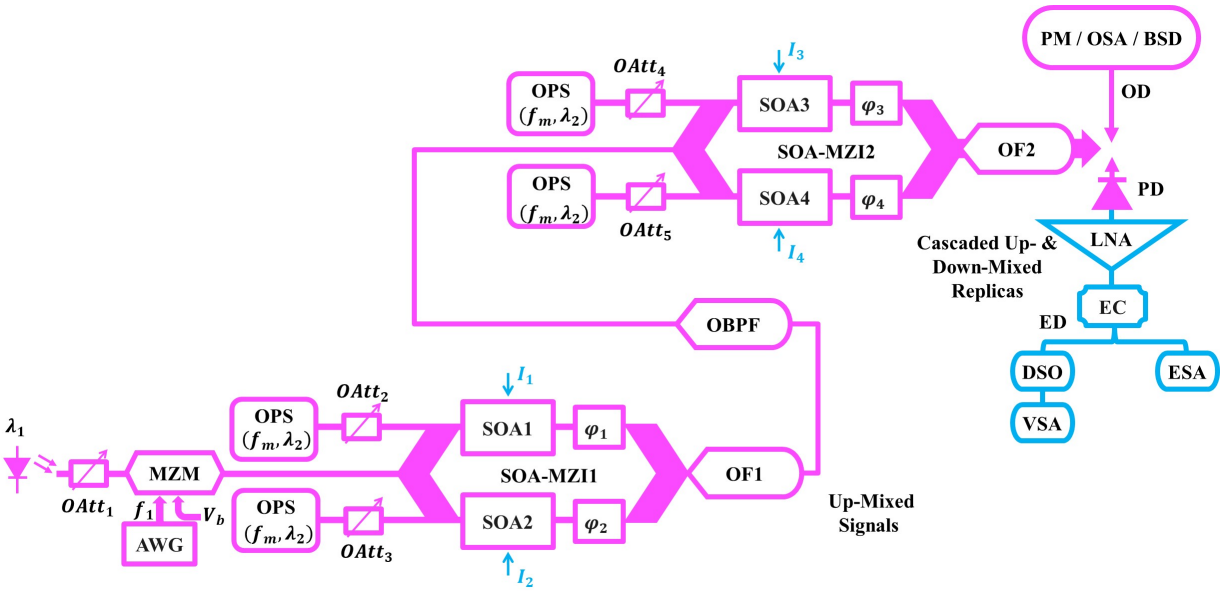


Figure 15. Experimental configuration of the differential all-optical cascaded system, with the singular deviation from the depiction in Figure 11 being the optical injection of all OPS signals at both the lower and upper SOAs within each SOA-MZI.

https://doi.org/10.64897/ieet.2026v2i1.001

In our investigations, we showcase the electrical frequency patterns of simultaneous upward and downward mixed duplicates at the outcome of the SOA-MZI2, as depicted in Figure 16 and Figure 17. These spectrum display serves as verification of the foundational concept underlying the all-optical and electro-optical distinct modulation designs, facilitating simultaneous up- and down-shifts within a frequency span of up to $10f_m + 5f_m + f_1 = 235$ GHz. Notably, the original input data signals undergo up-shifts at mixing frequencies $qf_m + 5f_m + f_1$ and down-shifts at $|5f_m + f_1 - qf_m|$. Consequently, the electro-optical differential configuration exhibits improved signal-to-noise ratio, enhanced harmonic suppression, and reduced nonlinear distortion compared to the all-optical differential configuration, particularly at high mixing frequencies where carrier-dynamics limitations become dominant.

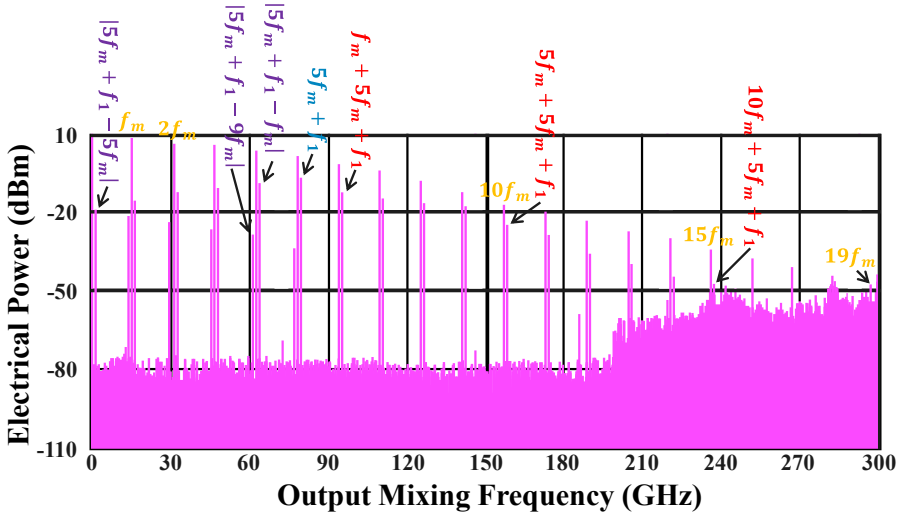


Figure 16. Electrical spectrum of the differential electro-optical cascaded system at the output of the SOA-MZI2.

The simultaneous transmissions, derived from the effective nonlinearities impact in the cascaded arrangement, diminish due to the constraints imposed by the SOA-MZI at elevated frequencies in the result of the successive setup. It is feasible to assess the efficiency by gauging all indicators mentioned earlier, encompassing intensity amplification, OCG, intensity steadiness beam quality coefficient, ECG, and EVM. Although the electrical frequency patterns are sufficient for scrutinizing the system efficiency and substantiating the expounded principle, the signal to noise ratio (SNR) of the simultaneous signal is gauged to scrutinize the efficiency for both sequenced systems.

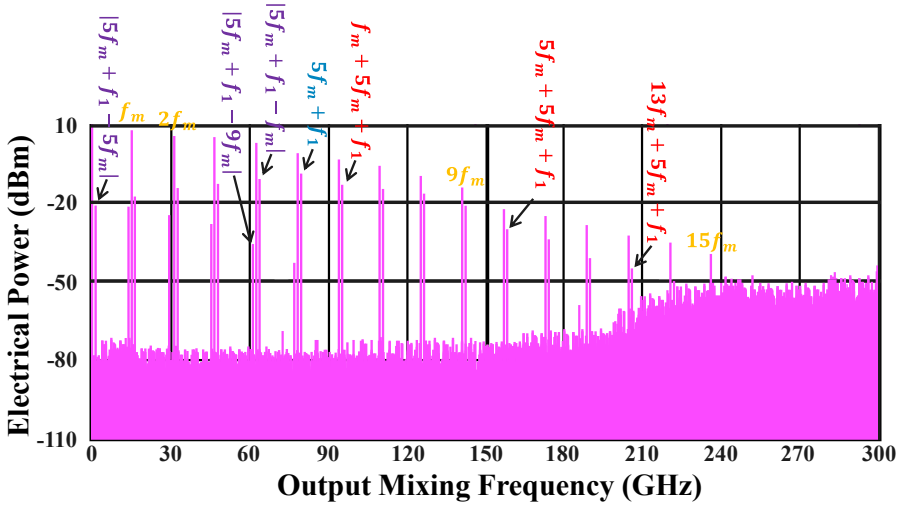


Figure 17. Electrical spectrum of the differential all-optical cascaded system at the output of the SOA-MZI2.

In optical experiments involving both all-optical and electro-optical configurations, we evaluate the excellence of the up- and down-mixed duplicates at the sequential SOA-MZIs output by gauging the SNR at each duplicate frequency. The SNR is assessed concerning the concurrent up- and down-blended signal at several output mixing frequencies, as depicted

in Figure 18 and Figure 19, respectively. It diminishes from 70 dB at 94.6 GHz to 9 dB at 235 GHz for electro-optical up-conversion and from 58 dB at 94.6 GHz to 0 dB at 235 GHz for all-optical up-conversion, as seen in Figure 18.

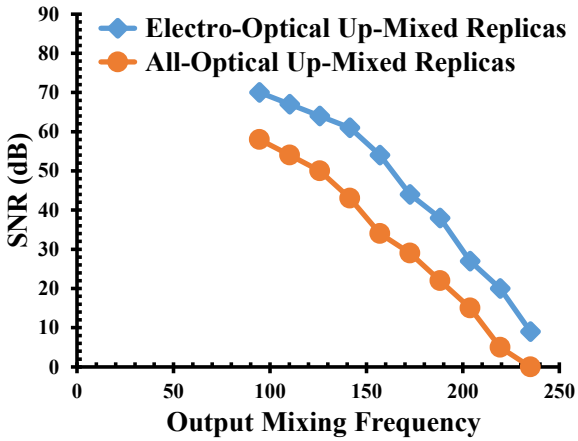


Figure 18. SNR of the all-optical and electro-optical up-converted replicas at the SOA-MZI2 output.

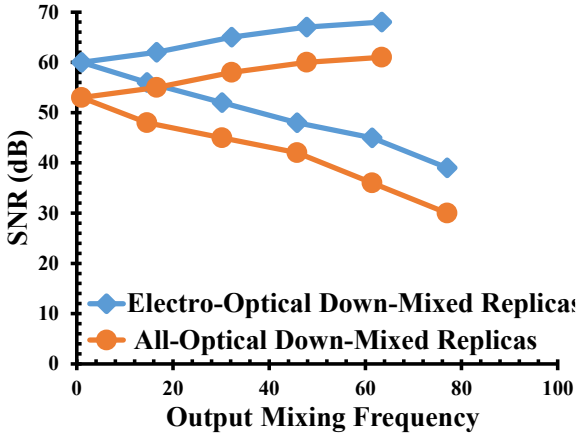


Figure 19. SNR of the all-optical and electro-optical down-converted replicas at the SOA-MZI2 output.

Similarly, it decreases from 68 dB at 63.4 GHz to 39 dB at 77 GHz for electro-optical down-conversion and from 61 dB at 63.4 GHz to 30 dB at 77 GHz for all-optical down-conversion, as observed in Figure 19. The decline in SNR with frequency is linked to the dynamic attributes of the employed SOA-MZI. As a result, the SNR values as well as the electrical spectrums affirm the superior efficacy of the electro-optical differential system.

7. Linewidth Characterization of All-Optical and Electro-Optical Concurrent Mixed Signals Using Standard and Differential Modulation Modes

Interference is essential in analyzing and controlling the linewidth of concurrent mixed signals. The interferometer's primary role in this configuration is to suppress frequency drift, which could otherwise compromise the precision of linewidth measurements. By introducing a defined time delay, the interferometric method translates frequency fluctuations into measurable intensity variations.

As illustrated in Figure 20, each cascaded mixing system is divided into two paths. One arm includes an optical fiber of length up to $L = 75$ km, which introduces a controlled temporal delay. The resulting phase difference between the two arms arises from this delay. After recombination, the optical signals are converted into electrical signals by a PD, and an ESA is used to evaluate the linewidth across modulation frequencies up to 1 GHz.

Alternative interferometric schemes [34–36] typically involve phase modulation in one arm and a passive fiber delay in the other, creating asymmetric phase shifts for linewidth analysis. However, in this study, since modulation is already present in the cascaded mixing systems, additional phase modulation is avoided to prevent undesired side effects.

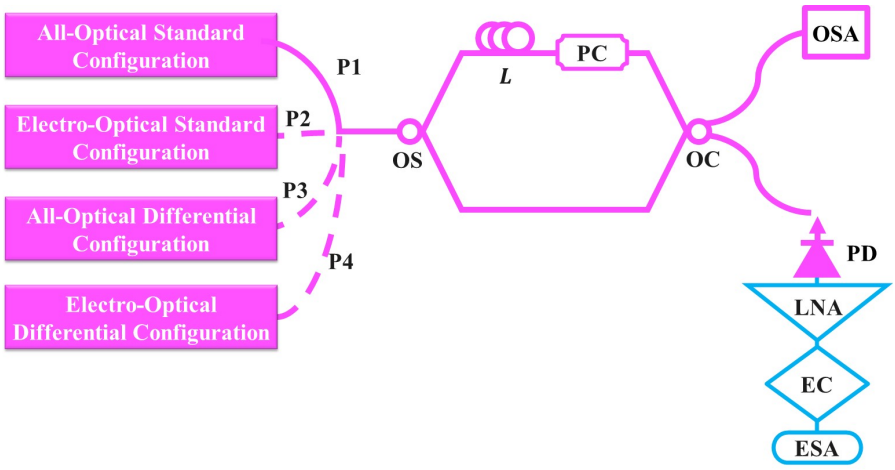


Figure 20. Schematic of the interferometric linewidth measurement of the concurent mixed signal based on the cascaded SOA-MZIs using all-optical standard configuration at port 1 (P1), electro-optical standard configuration at P2, all-optical differential configuration at P3, and electro-optical differential configuration at P4. The system includes optical fiber of length *L*, a polarisation controller (PC), an optical splitter (OS), and an optical coupler (OC).

The linewidth broadening mechanism in cascaded SOA-MZI systems is strongly influenced by carrier-density fluctuations, spontaneous emission noise, and modulation-induced refractive index variations. The coherence time of the generated optical signal is inversely proportional to the spectral linewidth and can be expressed as:

$$\Delta\nu = \frac{1}{\pi\tau_c} \tag{7}$$

where $\Delta\nu$ is the linewidth and τ_c is the coherence time. As the modulation frequency increases, rapid carrier-density oscillations inside the SOAs generate stronger phase fluctuations, thereby increasing spectral broadening.

Figure 21 shows how the linewidth of these four configurations varies with modulation frequency, ranging from 50 MHz to 1 GHz. Overall, the linewidth increases with modulation frequency, indicating the influence of modulation-induced phase noise and carrier dynamics. Among all systems, the electro-optical differential configuration consistently demonstrates the narrowest linewidth, suggesting better suppression of gain-induced phase fluctuations and spontaneous emission noise. On the other hand, the all-optical standard configuration exhibits the broadest linewidth, which indicates increased phase noise and reduced frequency stability.

At 50 MHz, the lowest linewidths are recorded for all configurations. At 1 GHz, the measured linewidths are: 280 kHz for the all-optical standard configuration, 210 kHz for the electro-optical standard configuration, 150 kHz for the all-optical differential configuration, and 80 kHz for the electro-optical differential configuration. These measurements provide insight into the noise characteristics and frequency stability of each system under different modulation conditions.

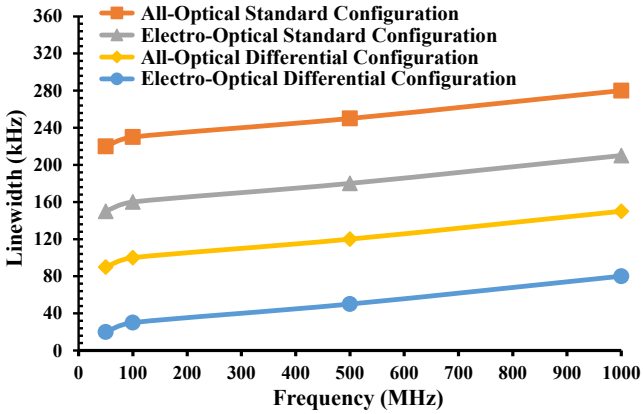


Figure 21. Measured linewidth of the four cascaded mixed systems for different modulation frequencies.

The primary cause of linewidth broadening is attributed to fluctuations in carrier density and refractive index variations within the SOA-MZI. As modulation frequency increases, these dynamic changes induce phase noise, leading to broader spectral lines. The interferometric setup effectively filters out low-frequency drifts while retaining high-frequency components, enabling accurate linewidth analysis. The superior performance of the electro-optical differential configuration points to an optimized design, offering reduced spontaneous emission noise, improved gain compression, and enhanced feedback control. These features make it an excellent candidate for applications requiring ultra-narrow linewidth and high-frequency stability.

In cascaded SOA-MZI structures, ASE noise accumulation becomes increasingly significant due to successive amplification stages. This accumulated ASE contributes directly to phase noise enhancement and linewidth broadening, particularly in the all-optical configurations where optical nonlinear interactions dominate.

The measured beat spectrum was fitted using a **Lorentzian profile**, and the corresponding FWHM was used to determine the laser linewidth. All linewidth measurements were performed under identical experimental conditions for the four investigated configurations to ensure a consistent comparison. The observed linewidth reduction is attributed to improved carrier-density stability and reduced ASE accumulation in the cascaded SOA-MZI architecture. This interpretation is qualitative and is consistent with the established physical behavior of SOA-based photonic devices.

To ensure a fair comparison between the investigated configurations, all measurements were carried out under identical experimental conditions. The input optical power, RF driving power, receiver configuration, measurement bandwidth, and instrument settings were maintained unchanged throughout all experiments. The reported results correspond to repeated stable measurements, and the same acquisition procedure was applied to all investigated configurations.

8. Comparative Performance Analysis of the Proposed Cascaded SOA-MZI Configurations

To provide a comprehensive comparison of the proposed dual SOA-MZI architectures, the experimental performance of the four investigated configurations is summarized in Table 8. All measurements were performed under identical experimental conditions, including the same input optical power, RF driving conditions, measurement bandwidth, receiver settings, and acquisition procedure, thereby ensuring a fair and unbiased comparison. While the preceding sections discuss the principal performance parameters relevant to each individual investigation, Table 8 consolidates all experimentally measured performance metrics into a single comparison. Additional measured parameters are included for completeness to provide an overall assessment of the four proposed configurations while avoiding unnecessary repetition throughout the manuscript.

Table 8. Comprehensive experimental comparison of the four investigated cascaded SOA-MZI configurations under identical operating conditions.

Simultaneous Up and Down Conversion Based on the Cascaded SOA-MZIs				
Performance Parameter	**All-Optical Standard**	**Electro-Optical Standard**	**All-Optical Differential**	**Electro-Optical Differential**
Maximum Frequency Range (GHz)	235	235	235	**235**
Maximum Output Optical Power (dBm)	23.0	28.8	27.8	33.2
OCG (dB)	33.0	38.8	37.8	43.2
Maximum ECG (dB)	8.4	14.5	13.5	20.5
Beam quality (M^2)	1.45	1.20	1.29	1.1
Maximum Harmonic distortion (%)	9	6.7	3.5	2
Linewidth (kHz)	280	210	150	**80**
OFDM modulation formats	OFDM-16-QAM	OFDM-1024-QAM	OFDM-16-QAM	OFDM-1024-QAM
Maximum data rate (Gbit/s)	1.39	6.96	1.39	6.96
Minimum EVM (%)	16	1.5	10	**0.25**
RMS power stability (%)	2	1.5	1.6	**0.66**
Maximum SNR (dB)	60	62	61	**70**

As summarized in Table 8, the electro-optical configurations consistently provide higher output optical power, OCG, ECG, beam quality, and SNR than their corresponding all-optical counterparts. Furthermore, the application of differential modulation significantly improves the performance of both architectures by reducing harmonic distortion, narrowing the

linewidth, improving power stability, and lowering the EVM. Among the four investigated configurations, the electro-optical differential configuration achieves the highest measured output optical power of 33.2 dBm, OCG of 43.2 dB, ECG of 20.5 dB, beam quality of $M^2 = 1.1$, maximum SNR of 70 dB, and RMS power stability of 0.66%, while simultaneously providing the lowest linewidth of 80 kHz, harmonic distortion of 2%, and EVM of 0.25%. These results demonstrate the benefits of combining electro-optical operation with differential modulation for simultaneous optical frequency up- and down-conversion using cascaded SOA-MZI architectures.

It is worth noting that all values reported in Table 8 were obtained experimentally under identical operating conditions. The table summarizes the complete experimental characterization of the four proposed configurations. Some performance metrics are presented here for completeness and comparative assessment and are therefore not discussed individually in the preceding sections.

9. Comparison with State of the Art

To evaluate the significance of the proposed cascaded SOA-MZI architectures, a comparison with previously reported SOA-MZI-based photonic mixing systems is presented in Table 9. The comparison includes the system architecture, maximum operational frequency, modulation format, conversion performance, EVM, BR, linewidth characterization, and principal contribution of each work.

Previous studies primarily focused on either up-conversion or down-conversion using single-stage SOA-MZI structures, while limited attention has been devoted to simultaneous concurrent up and down conversion using cascaded architectures. Furthermore, linewidth characterization and frequency-stability analysis are rarely investigated in SOA-MZI photonic mixers.

Compared to earlier works, the proposed electro-optical differential cascaded SOA-MZI system demonstrates several advantages, including simultaneous up- and down-frequency conversion, operation up to 235 GHz, enhanced optical and electrical conversion gains, reduced harmonic distortion, improved EVM performance, compatibility with OFDM-1024-QAM transmission, and linewidth reduction down to 80 kHz. These results confirm that the proposed differential electro-optical cascaded architecture provides improved nonlinear mixing efficiency, enhanced spectral stability, and superior signal quality compared with previously reported SOA-MZI mixing systems.

Table 9. Comparison between previously reported SOA-MZI mixing systems and the proposed cascaded architectures.

Ref.	Architecture	Mixing Type	Maximum Frequency	Modulation Format	Conversion Gain (dB)	EVM (%)	BR	Linewidth Characterization
[7]	Single SOA-MZI	Down conversion	22.5 GHz	PSK	1.5	NO	1.55 Mbit/s	No
[5]	Electro-optical SOA-MZI	Up conversion	59 GHz	QPSK	34	5.5	5 Gbit/s	No
[6]	Differential electro-optical SOA-MZI	Up conversion	118.5 GHz	128-QAM	38.7	6	70 Gbit/s	No
[37]	All-Optical SOA-MZI	Up/down Conversion	22.5 GHz	No	13.2	NO	NO	No
[38–41]	Parallel SOA-MZIs	Wavelength conversion	86.3 GHz	QPSK	8	18	40.5 Gbit/s	No
[15]	Parallel SOA-MZIs	Down conversion	99 GHz	OFDM	25	29	2 Gbit/s	No
This Work	Dual-cascaded all-optical and electro-optical SOA-MZIs	Simultaneous up and down conversion	235 GHz	OFDM-1024-QAM	14.5	0.25	6.96 Gbit/s	80 kHz

As summarized in Table 9, previously reported SOA-MZI photonic mixing systems mainly focused on either up-conversion or down-conversion using single-stage or parallel configurations without detailed linewidth characterization [5,7,13,15]. The cascaded SOA-MZI arrangement demonstrated simultaneous up/down conversion through simulation analysis only, without experimental linewidth evaluation. In contrast, the present work experimentally demonstrates

a dual-cascaded SOA-MZI architecture capable of simultaneous up- and down-frequency conversion over an extended operational frequency range reaching 235 GHz. Furthermore, the proposed electro-optical differential configuration achieves enhanced electrical and optical conversion gains, reduced harmonic distortion, improved EVM performance for OFDM-1024-QAM transmission, and linewidth narrowing down to 80 kHz. Unlike previous studies [5,6,13,17], this work additionally investigates linewidth evolution as a function of modulation frequency, providing deeper insight into phase-noise behavior and spectral stability in cascaded SOA-MZI photonic mixers. These results confirm the advantages of the proposed electro-optical differential architecture for high-frequency microwave photonic applications requiring improved coherence, frequency stability, and nonlinear mixing efficiency.

Unlike previous studies, the present work introduces linewidth characterization as an additional evaluation metric for cascaded SOA-MZI photonic mixers. The obtained results demonstrate that electro-optical differential modulation significantly improves spectral coherence and suppresses phase-noise-induced broadening. In addition, the proposed architecture achieves improved harmonic suppression and enhanced OFDM transmission quality at millimeter-wave frequencies.

Despite the significant improvements achieved by the proposed electro-optical differential cascaded SOA-MZI system, several limitations remain. The performance at very high frequencies is constrained by the carrier recovery time and nonlinear bandwidth of the SOAs. In addition, ASE accumulation through the cascaded amplification stages contributes to linewidth broadening and degradation of high-order harmonic replicas. Future work may focus on integrating low-noise SOAs, optimized phase-control mechanisms, photonic integration platforms to further enhance frequency stability and extend the operational bandwidth toward the terahertz regime, and applying linewidth reduction on the mixing system.

10. Conclusions

In this work, we evaluated outstanding all-optical and electro-optical topologies employing an OFDM transmission cascaded SOA-MZIs system. The experimental findings demonstrated the feasibility of implementing an OFDM data transmission cascade system. This can happen after examining the effect of the OPS signal location with regard to cyclic prefix and bias current elements on the mixing procedure. The EVM, ECG, OCG, and M^2 measurements indicated that the electro-optical technique, as compared to the all-optical procedure, could greatly enhance the performance evaluation of the cascaded SOA-MZIs system, particularly when adjusting the selectivity of required operational parameters. At a CP of 10%, the electro-optical technique resulted in an EVM improvement of roughly 6% in comparison with the all-optical concept, from 18 to 12% for up-conversion and from 16 to 10% for down-conversion. Furthermore, the methodologies suggested in this work have the possibility of being extended to higher-order M-QAM formats, allowing for larger bit rates and enhancing overall cascaded system performance. In contrast to the all-optical cascaded approach, the ECG of the up- and down-mixed signal upgrades by 6 dB over the entirety of the mixing frequency interval for the electro-optical cascaded network. Furthermore, the greatest frequency range for up- and down-shifting is 235 and 77 GHz, respectively. The experimental cascaded SOA-MZI setup has been proven to deliver simultaneous average powers of up to 23 and 28.8 dBm for all-optical and electro-optical designs, respectively, at 1550 nm for an incoming signal power of −10 dBm and an OPS power of 5 dBm. This corresponds to an OCG of 33 dB for the all-optical design and 38.8 dB for the electro-optical arrangements. The final output, which corresponds to the concurrent up- and down-mixed signal from cascaded SOA-MZIs, exhibits excellent circularity and M^2 measurements, particularly for the electro-optical approach, up to higher than 95% and less than 1.2, respectively. The adoption of an electro-optical cascaded system could not only benefit the amplification stage but also help reduce the strong noise while operating in the SOAs high-gain limit. The linewidth investigation further demonstrated that electro-optical differential modulation significantly improves spectral coherence and frequency stability by mitigating gain-induced phase fluctuations and nonlinear noise accumulation inside the cascaded SOA-MZI structure. These findings establish linewidth characterization as an additional performance metric for evaluating advanced photonic mixing systems. Finally, the employment of differential mode depending on the electro-optical cascaded system strengthens its performance features because of its higher signal power, noise reduction, lowest linewidth, compensation for nonlinear distortions higher modulation bandwidths, and faster response times.

Author Contributions: The authors Hassan Termos and Kassem Kallas contributed to this paper. They read and agreed to the published version of the manuscript.

Funding: This research received no external funding.

Data Availability Statement: Data underlying the results presented in this paper are not publicly available at this time but may be obtained from the authors upon reasonable request.

Conflicts of Interest: The authors declare no conflict of interest.

Abbreviations

ASE	Amplified Spontaneous Emission
AWG	Arbitrary Waveform Generator
BR	Bit Rate
CP	Cyclic Prefix
DSO	Digital Sampling Oscilloscope
ECG	Electrical Conversion Gain
ED	Electrical Domain
ESA	Electrical Spectrum Analyzer
EVM	Error Vector Magnitude
FEC	Forward Error Correction
FWHM	Full Width at Half Maximum
LNA	Low Noise Amplifier
MZM	Mach–Zehnder Modulator
OCG	Optical Conversion Gain
OD	Optical Domain
OFDM	Orthogonal Frequency Division Multiplexing
OF	Optical Filter
OSA	Optical Spectrum Analyzer
OPS	Optical Pulse Source
OS	Optical Splitter
PSK	Phase Shift Keying
PD	Photodetector
PM	Power Meter
QPSK	Quadrature Phase Shift Keying
RMS	Root Mean Square
RoF	Radio over Fiber
SOA	Semiconductor Optical Amplifier
SOA-MZI	Semiconductor Optical Amplifier Mach–Zehnder Interferometer
SNR	Signal-to-Noise Ratio
SR	Symbol Rate
VSA	Vector Signal Analyzer
WDM	Wavelength Division Multiplexing
XGM	Cross-Gain Modulation
XPM	Cross-Phase Modulation

References

[1] N. J. Gomes, P. P. Monteiro, and A. Gameiro, Eds., *Next Generation Wireless Communications Using Radio over Fiber*. Chichester, U.K.: John Wiley & Sons, Oct. 2012. [CrossRef]

[2] G. H. Smith, D. Novak, and C. Lim, "A millimeter-wave full-duplex fiber-radio star-tree architecture incorporating WDM and SCM," *IEEE Photon. Technol. Lett.*, vol. 10, no. 11, pp. 1650–1652, Nov. 1998. [CrossRef]

[3] R. G. Vaughan, N. L. Scott, and D. R. White, "The theory of bandpass sampling," *IEEE Trans. Signal Process.*, vol. 39, no. 9, pp. 1973–1984, Sep. 1991. [CrossRef]

[4] H. Termos and A. Mansour, "Concurrent m-QAM transmission performance assessment in a combined four SOA-MZIs arrangement," *Opt. Lasers Eng.*, vol. 176, May 2024, art. no. 108110. [CrossRef]

[5] H. Termos and A. Mansour, "Frequency alteration built on an electro-optical sampling SOA−MZI using a differential modulation schema," *Optics*, vol. 3, no. 3, pp. 225–233, Jul. 2022. [CrossRef]

[6] H. Termos, A. Mansour, and M. Ebrahim-Zadeh, "Establishment of an electro-optical mixing design on a photonic SOA-MZI using a differential modulation arrangement," *Sensors*, vol. 23, no. 9, Apr. 2023, art. no. 4380. [CrossRef]

[7] H.-J. Song and J.-I. Song, "Simultaneous all-optical frequency downconversion technique utilizing an SOA-MZI for WDM radio over fiber (RoF) applications," *J. Lightw. Technol.*, vol. 24, no. 8, pp. 3028–3034, Aug. 2006. [CrossRef]

[8] J. A. Summers, M. L. Masanovic, V. Lal, and D. J. Blumenthal, "Design and operation of a monolithically integrated two-stage tunable all-optical wavelength converter," *IEEE Photon. Technol. Lett.*, vol. 19, no. 16, pp. 1248–1250, Aug. 2007. [CrossRef]

[9] H. Termos and A. Mansour, "All-optical three-input "AND" gate dependent on a differential modulation architecture," *Electronics*, vol. 12, no. 7, Mar. 2023, art. no. 1510. [CrossRef]

[10] H. Termos and A. Mansour, "High-repetition-rate femtosecond "OR" gate design in a differential SOA-MZI," *Optik*, vol. 304, Jun. 2024, art. no. 171760. [CrossRef]

[11] H. Termos and K. Kallas, "Performance characterizations of a simultaneous "AND" - "OR" gates system dependent on a parallel-series SOA-MZIs combination," *J. Electron. Electr. Eng.*, vol. 5, no. 1, pp. 181–202, May 2026. [CrossRef]

[12] H. Termos, "Study of up & down conversion technique by all-optical sampling based on SOA-MZI," Ph.D. dissertation, Univ. de Bretagne Occidentale, Brest, France, Feb. 2017. [CrossRef]

[13] H. Termos, A. Mansour, and A. Nasser, "Simultaneous up-conversion based on a co- & counter-directions SOA-MZI sampling mixer with standard & differential modulation modes," *Photonics*, vol. 9, no. 2, Feb. 2022, art. no. 109. [CrossRef]

[14] H. Termos and A. Mansour, "OFDM signal down frequency conversion based on a SOA-MZI sampling mixer using differential modulation and switching architectures," *Optik*, vol. 245, Nov. 2021, art. no. 167761. [CrossRef]

[15] H. Termos and A. Mansour, "Sampling parallel SOA-MZIs configuration for all-optical simultaneous frequency down-conversion," *Photonics*, vol. 9, no. 10, Oct. 2022, art. no. 745. [CrossRef]

[16] H. Termos and A. Mansour, "SOA-MZI differential transformation approach applied on simultaneous electro-optical mixing," *Photonics*, vol. 10, no. 6, Jun. 2023, art. no. 649. [CrossRef]

[17] H. Termos, A. Mansour, and A. Nasser, "Simultaneous up- and down-frequency mixing based on a cascaded SOA-MZIs link," *Appl. Opt.*, vol. 60, no. 27, pp. 8336–8348, Sep. 2021. [CrossRef]

[18] G. Qi, J. Yao, J. Seregelyi, S. Paquet, and J. C. Bélisle, "Effects of amplified spontaneous emission noise of optical amplifiers on the phase noise of optically generated electrical signals," in *Proc. SPIE, Photonic Applications in Nonlinear Optics, Nanophotonics, and Microwave Photonics*, vol. 5971, Toronto, Canada, Sep. 2005, paper 59712D. [CrossRef]

[19] A. Fernandez, L. Chao, and J. W. D. Chi, "All-optical clock recovery and pulse reshaping using semiconductor optical amplifier and dispersion compensating fiber in a ring cavity," *IEEE Photon. Technol. Lett.*, vol. 20, no. 13, pp. 1148–1150, Jul. 2008. [CrossRef]

[20] V. Stasyuk, *Test Data and Operation Manual of Ultrafast Optical Clock*, PriTel, Inc., Naperville, IL, USA, accessed: Jun. 23, 2023. [Online]. Available: https://www.pritel.com

[21] K. S. Giboney, M. J. W. Rodwell, and J. E. Bowers, "Traveling-wave photodetector theory," *IEEE Trans. Microw. Theory Techn.*, vol. 45, no. 8, pp. 1310–1319, Aug. 1997. [CrossRef]

[22] T. Nagatsuma, H. Ito, and T. Ishibashi, "High-power RF photodiodes and their applications," *Laser Photon. Rev.*, vol. 3, pp. 123–137, Feb. 2009. [CrossRef]

[23] H. Ito, T. Furuta, S. Kodama, and T. Ishibashi, "InP/InGaAs uni-travelling-carrier photodiode with 310 GHz bandwidth," *Electron. Lett.*, vol. 36, no. 21, pp. 1809–1810, Oct. 2000. [CrossRef]

[24] D. Wright, "Beamwidths of a diffracted laser using four proposed methods," *Opt. Quantum Electron.*, vol. 24, no. 9, pp. S1129–S1135, Sep. 1992. [CrossRef]

[25] A. E. Siegman, "How to (Maybe) measure laser beam quality," in *DPSS (Diode Pumped Solid State) Lasers: Applications and Issues*, ser. OSA Trends in Optics and Photonics, M. Dowley, Ed., vol. 17. Washington, D.C.: Optical Society of America, 1998, paper MQ1. [CrossRef]

[26] R. Schmogrow, B. Nebendahl, M. Winter, A. Josten, D. Hillerkuss, S. Koenig, J. Meyer, M. Dreschmann, M. Huebner, C. Koos, J. Becker, W. Freude, and J. Leuthold, "Error vector magnitude as a performance measure for advanced modulation formats," *IEEE Photon. Technol. Lett.*, vol. 24, no. 1, pp. 61–63, Jan. 2012. [CrossRef]

[27] R. P. Schreieck, M. H. Kwakernaak, H. Jackel, and H. Melchior, "All-optical switching at multi-100-Gb/s data rates with Mach-Zehnder interferometer switches," *IEEE J. Quantum Electron.*, vol. 38, no. 8, pp. 1053–1061, Aug. 2002. [CrossRef]

[28] C. Schubert, J. Berger, S. Diez, H. J. Ehrke, R. Ludwig, U. Feiste, C. Schmidt, H. G. Weber, G. Toptchiyski, S. Randel, and K. Petermann, "Comparison of interferometric all-optical switches for demultiplexing applications in high-speed OTDM systems," *J. Lightw. Technol.*, vol. 20, no. 4, pp. 618–624, Apr. 2002. [CrossRef]

[29] D. Shmilovitz, "On the definition of total harmonic distortion and its effect on measurement interpretation," *IEEE Trans. Power Del.*, vol. 20, no. 1, pp. 526–528, Jan. 2005. [CrossRef]

[30] *LTE; Evolved Universal Terrestrial Radio Access (E-UTRA); Base Station (BS) Radio Transmission and Reception*, 3GPP Std. TS 36.104, Rev. V14.3.0, Release 14 (ETSI TS 136 104), Apr. 2017, accessed: Aug. 11, 2023. [Online]. Available: https://www.etsi.org/deliver/etsi_ts/136100_136199/136104/14.03.00_60/ts_136104v140300p.pdf

[31] D.-N. Nguyen, J. Bohata, J. Spacil, D. Dousek, M. Komanec, S. Zvanovec, Z. Ghassemlooy, and B. Ortega, "M-QAM transmission over hybrid microwave photonic links at the K-band," *Opt. Express*, vol. 27, no. 23, pp. 33 745–33 756, Nov. 2019. [CrossRef]

[32] E. McCune, "Precision and efficient 1024-QAM transmitter based on the switch-mode mixer modulator," in *Proc. IEEE Radio and Wireless Symp. (RWS)*, Orlando, FL, USA, Jan. 2019, pp. 1–4. [CrossRef]

[33] E. McCune and Q. Diduck, "4096-QAM microwave transmitter providing efficiency exceeding 50% and EVM below 1%," in *Proc. 49th Eur. Microwave Conf. (EuMC)*, Paris, France, Oct. 2019, pp. 896–899. [CrossRef]

[34] H. Ludvigsen, M. Tossavainen, and M. Kaivola, "Laser linewidth measurements using self-homodyne detection with short delay," *Opt. Commun.*, vol. 155, no. 1–3, pp. 180–186, Oct. 1998. [CrossRef]

[35] P. Horak and W. H. Loh, "On the delayed self-heterodyne interferometric technique for determining the linewidth of fiber lasers," *Opt. Express*, vol. 14, no. 9, pp. 3923–3928, May 2006. [CrossRef]

[36] Z. Zhao, Z. Bai, D. Jin, Y. Qi, J. Ding, B. Yan, Y. Wang, Z. Lu, and R. P. Mildren, "Narrow laser-linewidth measurement using short delay self-heterodyne interferometry," *Opt. Express*, vol. 30, no. 17, pp. 30 600–30 610, Aug. 2022. [CrossRef]

[37] H.-J. Song, J. S. Lee, and J.-I. Song, "All-optical harmonic frequency up-conversion for a WDM radio over fiber system," in *Proc. IEEE MTT-S Int. Microwave Symp. Dig.*, vol. 1, Fort Worth, TX, USA, Jun. 2004, pp. 405–407. [CrossRef]

[38] K. Mishina, S. M. Nissanka, A. Maruta, S. Mitani, K. Ishida, K. Shimizu, T. Hatta, and K.-i. Kitayama, "All-optical modulation format conversion from NRZ-OOK to RZ-QPSK using parallel SOA-MZI OOK/BPSK converters," *Opt. Express*, vol. 15, no. 12, pp. 7774–7785, Jun. 2007. [CrossRef]

[39] J. P. Turkiewicz, "All-optical OOK-to-QAM modulation format conversion utilizing parallel SOA-MZI wavelength converters," *Microw. Opt. Technol. Lett.*, vol. 54, no. 10, pp. 2429–2433, Oct. 2012. [CrossRef]

[40] K. Mishina, T. Kono, A. Maruta, and K.-i. Kitayama, "All-optical OOK-to-16QAM format conversion by using SOA-MZI wavelength converters," in *Proc. 17th Opto-Electron. Commun. Conf. (OECC)*, Busan, Korea (South), Jul. 2012, pp. 337–338. [CrossRef]

[41] K. Mishina, D. Hisano, and A. Maruta, "All-optical modulation format conversion and applications in future photonic networks," *IEICE Trans. Electron.*, vol. E102.C, no. 4, pp. 304–315, Apr. 2019. [CrossRef]